CELLULAR NEUROSCIENCE

GABA signaling triggered by TMC-1/Tmc delays neuronal aging by inhibiting the PKC pathway in *C. elegans*

Jieyu Wu[1], Liuyang Wang[1], John F. Ervin[2], Shih-Hsiu J. Wang[3], Erik Soderblom[4], Dennis Ko[1,5], Dong Yan[1,6]*

Aging causes functional decline and degeneration of neurons and is a major risk factor of neurodegenerative diseases. To investigate the molecular mechanisms underlying neuronal aging, we developed a new pipeline for neuronal proteomic profiling in young and aged animals. While the overall translational machinery is down-regulated, certain proteins increase expressions upon aging. Among these aging–up-regulated proteins, the conserved channel protein TMC-1/Tmc has an anti-aging function in all neurons tested, and the neuroprotective function of TMC-1 occurs by regulating GABA signaling. Moreover, our results show that metabotropic GABA receptors and G protein GOA-1/Goα are required for the anti-neuronal aging functions of TMC-1 and GABA, and the activation of GABA receptors prevents neuronal aging by inhibiting the PLCβ-PKC pathway. Last, we show that the TMC-1–GABA–PKC signaling axis suppresses neuronal functional decline caused by a pathogenic form of human Tau protein. Together, our findings reveal the neuroprotective function of the TMC-1–GABA–PKC signaling axis in aging and disease conditions.

INTRODUCTION

Aging is a universal phenomenon that markedly increases the probability of developing neurodegenerative diseases (*1*, *2*). By 2050, the proportion of the global population over 65 is projected to be 16%, with those aged 80 or more estimated to triple over the same timeframe (*3*). There is thus a critical need to better understand the molecular mechanisms underlying neuronal aging and aging-associated neurodegeneration.

Neuronal aging is a slow progressive change, taking decades in humans (average life span: 70 to 80 years), months in rodents (average life span: 2 to 3 years), and 1 to 2 weeks in *Caenorhabditis elegans* (average life span: 2 to 3 weeks) (*4*). Changes in protein profiles are believed to play a key role during this process (*5*). In the past decade, studies of mRNA profiling during aging in different model organisms have shed light on how aging affects gene expression in neurons (*6*). However, emerging evidence show that mRNA levels are not always correlated with protein levels, and in certain cases, mRNA and protein levels can be independent (*7*). Thus, to fully understand neuronal aging, it is important to reveal proteomic level changes in neurons.

In this study, we used the TurboID proximity labeling system (*8*) to develop a new pipeline for in vivo neuronal proteomic profiling in young and aged *C. elegans*. Our proteomic results show that most neuronal proteins have lower expression levels in aged animals when compared with young animals, but a small group of proteins increase in expression during aging. Among these proteins, we revealed the anti-degeneration and anti-neuronal aging functions of *tmc-1*, the *C. elegans* homolog of mammalian transmembrane channel–like (Tmc) channels. We further demonstrated that the anti-neuronal aging function of *tmc-1* is through control of γ-aminobutyric acid (GABA) release, which, in turn, suppresses neurodegeneration and neuronal aging through the metabotropic $GABA_B$ receptor GBB-1. The activation of GBB-1 activates the heterotrimeric guanine nucleotide–binding protein (G protein) GOA-1/Goα to inhibit the protein kinase C (PKC) pathway and protect neurons from aging-associated degeneration and functional decline. As most neurons that we examined do not have direct inputs from GABAergic neurons, our results emphasize the critical role of extrasynaptic GABA in neuronal aging. Moreover, we examined the neuroprotective function of TMC-1 in a *C. elegans* Alzheimer's disease model and show that activation of the TMC-1–GABA–PKC signaling axis can suppress neuronal functional decline caused by expression of a pro-aggregation fragment of the human Tau protein. Therefore, our study uncovers an unexpected anti-aging function of the conserved channel protein TMC-1/TMC and reveals the novel role of extrasynaptic GABA in regulating neuronal aging, aging-associated decline in axon regeneration, and aging- and disease-associated neurodegeneration and functional decline, which provides a new mechanism for neurodegeneration in physiological and pathological conditions.

The Tmc proteins are an evolutionarily conserved protein family that contains eight members in mammals. To date, most studies were focused on Tmc1 and Tmc2, where they have shown that these proteins are mainly expressed in the auditory system and are believed to be core components of the mechano-electrical transducer channel (*9*, *10*). However, Tmc proteins have a notable expression in many regions of the brain (Allen Brain Atlas, www.brain-map.org) (*11*), suggesting that they may play important

[1]Department of Molecular Genetics and Microbiology, Duke University Medical Center, Durham, NC 27710, USA. [2]Bryan Brain Bank and Biorepository, Department of Neurology, Duke University Medical Center, Durham, NC 27710, USA. [3]Department of Pathology & Department of Neurology, Duke University Medical Center, Durham, NC 27710, USA. [4]Proteomics and Metabolomics Shared Resource and Duke Center for Genomic and Computational Biology, Duke University Medical School, Durham, NC 27710, USA. [5]Division of Infectious Diseases, Department of Medicine, Duke University Medical Center, Durham, NC 27710, USA. [6]Department of Neurobiology, Regeneration Next, and Duke Institute for Brain Sciences, Duke University Medical Center, Durham, NC 27710, USA.
*Corresponding author. Email: dong.yan@duke.edu

roles outside the auditory system. In this study, we demonstrated that TMC channels function in GABAergic neurons to suppress neuronal aging in *C. elegans*.

In the brain, GABA plays a profound role as the primary inhibitory neurotransmitter (*12*). Unlike other neurotransmitters that are expressed at relatively low levels in the brain, GABA is abundant in the mammalian central nervous system and has been speculated to play other roles beyond being a neurotransmitter (*13*, *14*). In the human brain, the overall GABA level decreases upon aging, and this aging-associated GABA decline is tightly associated with degraded motor, visual, and cognitive performances in aged individuals (*15*, *16*). This aging-associated GABA decline was also observed in rodents and nonhuman primates, pointing out the potential evolutionarily conserved functions of GABA in neuronal aging (*17*, *18*). It has been found that an increase in GABA levels can reduce aging-associated neuronal functional decline in rodents and nonhuman primates (*19*). In addition, a decrease in GABA has also been observed in patients with various aging-associated neurodegenerative diseases (*20*). However, the function and regulation of GABA and GABA-associated signals in neuronal aging and neurodegeneration are still largely unclear.

GABA mainly acts through GABA receptors, including ionotropic $GABA_A$ and metabotropic $GABA_B$ receptors. $GABA_A$ receptors are GABA-gated chloride (Cl^-) channels that mediate fast responses by increasing the Cl^- permeability of the cell membrane to decrease neuron excitability (*21*); $GABA_B$ receptors are G protein–coupled receptors (GPCRs), which elicit slow and sustained activity by triggering signal transduction pathways via Gi/o proteins (*22*). While in the brain both ionotropic $GABA_A$ and metabotropic $GABA_B$ receptors function as receptors for GABA released from GABAergic neurons, they are also found to be expressed in many neurons that are not associated with GABAergic neurons (*23*, *24*). With the complete map of GABAergic neurons and GABA receptors, studies in *C. elegans* show that GABAergic neurons make up 10% of the total neuronal population, yet GABA receptors are expressed in nearly 90% of neurons, among which more than 31% of the $GABA_A$ and 37% of the $GABA_B$ receptor–expressing neurons are not associated with presynaptic GABAergic neurons (*25*, *26*). These studies suggest again that besides its role as a neurotransmitter, GABA may have important unknown extrasynaptic functions. Consistent with all these findings, we demonstrated the neuronal protective functions of GABA and GABA receptors in *C. elegans* and showed that extrasynaptic, rather than synaptic, GABA plays a critical role in regulating neuronal aging.

RESULTS

Proteomic profiling through in vivo TurboID labeling reveals aging-associated changes of protein levels

To examine the neuronal protein profiles of *C. elegans* at different ages, we took advantage of the recently developed TurboID proximity labeling system (*8*). TurboID is an engineered biotin ligase that can label proximal proteins with biotin on nucleophilic residues such as lysine (*8*). In previous studies, proximity labeling is commonly used to identify protein-protein interactions by attaching TurboID to a protein of interest. To examine the proteomic profile of neurons in vivo, we generated a transgene that expresses free TurboID in the *C. elegans* nervous system (Fig. 1A). Presumably, TurboID can freely distribute in neurons and randomly label all proteins with biotin. Neuronal proteins can then be enriched with streptavidin beads. To test this hypothesis, we first examined the distribution of free TurboID in neurons and confirmed that TurboID can distribute to all regions of neurons including soma, axons, and dendrites (Fig. 1A). Because *Escherichia coli* OP50, the strain conventionally used as a bacterial food source for *C. elegans*, expresses significant amounts of biotin, we used the biotin-auxotrophic *E. coli* strain MG1655 as a food source for TurboID-related experiments to lower the background labeling and to control the timing of the labeling. *C. elegans* fed with MG1655 for multiple generations at different temperatures have comparable life spans with animals grown in OP50 at each respective temperature (fig. S1, A and B), and no notable differences were observed between animals growing on MG1655 and OP50.

Next, we examined whether TurboID could efficiently label proteins with biotin in vivo. We carried out experiments using animals cultured at 20° or 25°C and provided 100 or 500 μM biotin at 2, 4, 6, or 8 hours before protein collection. We observed strong labeling of proteins only in animals cultured at 25°C, and the efficiency of labeling also depended on the time and concentration of biotin supplementation to animals (fig. S1, C and D). We further examined the labeling efficiency by providing biotin at different concentrations, ranging from 100 to 500 μM, for 8 hours and found that there was little difference among the 300, 400, and 500 μM groups (fig. S1E). Although TurboID is specifically expressed in neurons, it may also label proteins from other cells when animals are lysed during sample collection. To exclude this possibility, we examined whether adding biotin in the protein lysate could cause any labeling and found that no significant biotin labeling was observed by adding biotin after lysis (fig. S2A). Last, we determined that supplementation of 300 μM biotin to animals at 25°C 8 hours before sample collection can efficiently induce labeling of neuronal proteins, and by streptavidin bead enrichment, we can specifically probe for biotin-labeled proteins (fig. S2B). In conclusion, we have shown that expressing free TurboID in neurons while providing animals with the appropriate biotin concentrations and culturing temperatures can induce specific labeling of neuronal proteins.

As *C. elegans* neurons display certain aging phenotypes within 10 days of the adult stage (*27*, *28*), we decided to collect animals during days 1, 3, 6, 9, and 12 of adulthood (Fig. 1B). After streptavidin bead enrichment, we found that the labeling efficiency was similar at different ages, and all samples were then subjected to quantitative proteomics (fig. S2C). In each experiment, we used the wild-type N2 strain as an experimental negative control and performed receiver operating characteristic (ROC) analyses between experimental groups and their same-age negative N2 control counterparts. Results show specific enrichment of biotinylated proteins at all time points (Fig. 1C). We carried out three independent replicates of the neuronal proteomic experiments along with N2 controls, and R-squared analyses showed that each triplicate displayed almost identical results in both young and aged animals (Fig. 1, D and E). To uncover neuron-specific changes during aging, we also carried out similar analyses using two strains that express free TurboID in muscles and the hypodermis, respectively (fig. S2, D and E). Spearman correlation and principal components analysis show that the proteins identified in the three independent neuron-labeled replicates are clustered together and are clearly different from the muscle- or hypodermal-labeled samples (Fig. 1F

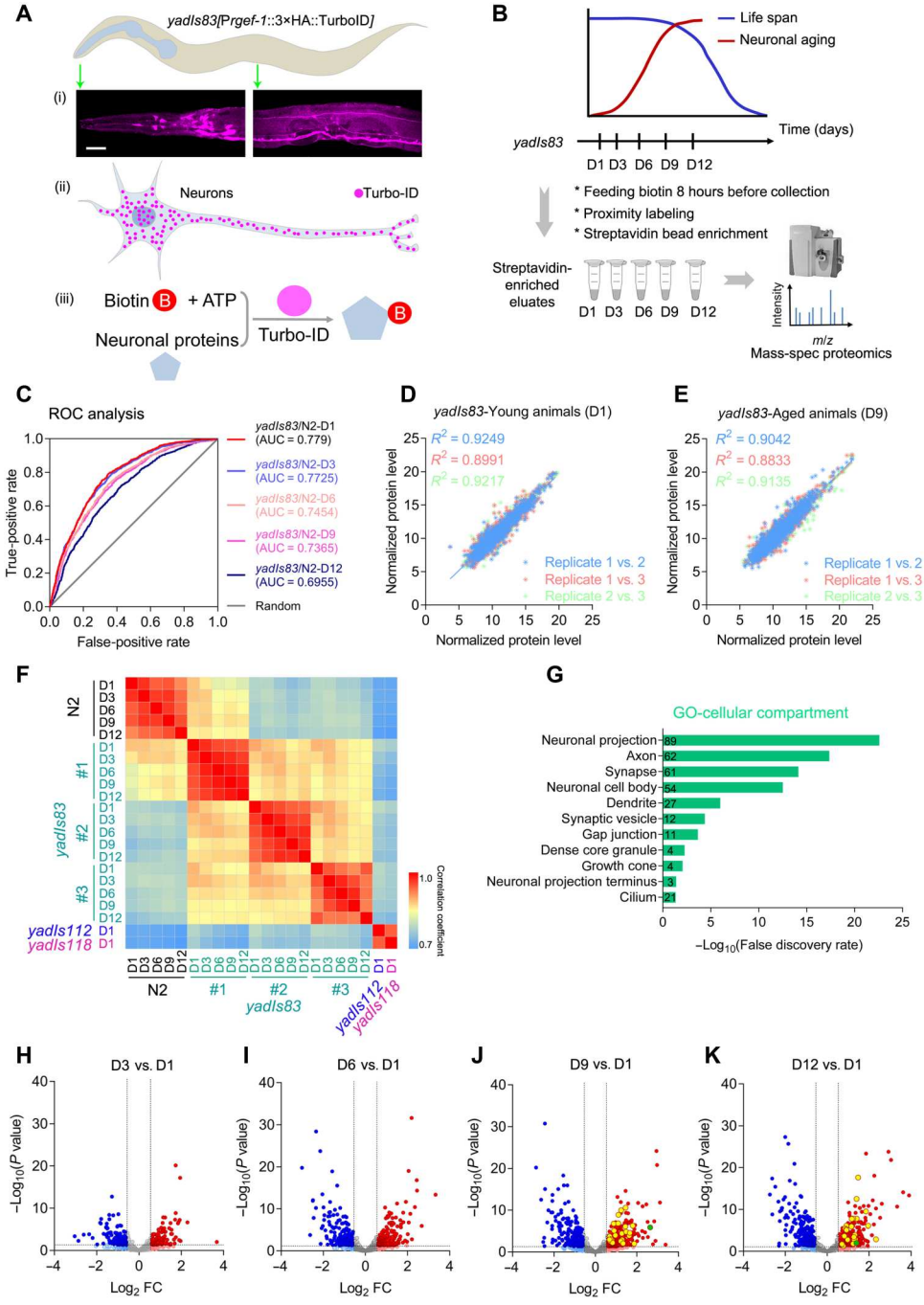

Fig. 1. Neuronal proteomic profiling reveals age-dependent change of protein levels. (**A**) Free TurboID is evenly distributed in *C. elegans* neurons. *yadIs83* [P*rgef-1*::3×HA::TurboID]: an integrated transgene expressing HA-tagged TurboID driven by a pan-neuronal promoter P*rgef-1*. (i) Image showing the distribution of HA-TurboID by immunostaining using anti-HA antibody; scale bar, 20 μm. (ii) Schematic diagram of the distribution of free TurboID. (iii) Summary of TurboID proximity labeling. (**B**) Scheme of TurboID-mediated proximity labeling at different ages. (**C**) Expression of free TurboID can specifically label neuronal proteins. The image shows the receiver operating characteristic (ROC) curve of each time point (days 1, 3, 6, 9, and 12). Wild-type N2 animals were used as negative controls for ROC analysis. Area under the curve (AUC) represents the degree of separability or specificity between experimental and control groups. (**D** and **E**) Data from correlation analysis (R^2) of the three biological replicates show high similarities in both young (D) and aged (E) animals. (**F**) Spearman correlation analyses show that neuronal proteomes exhibit high specificity when compared with proteomes from negative control N2 (wild-type strain), hypodermal, and muscle cells. *yadIs83*[P*rgef1*::3×HA::TurboID], neuronal expression of TurboID; *yadIs112*[P*col-19*::3×HA::TurboID], hypodermal expression of TurboID; *yadIs118*[P*myo-3*::3×HA::TurboID], muscle expression of TurboID. (**G**) Gene ontology analyses show that the results from neuronal proteomics uncover proteins expressed in all neuronal cellular compartments. The numbers on the bar indicate the gene number clustered on the term. (**H** to **K**) Volcano plots of proteomes show proteins with significant changes in day 3, 6, 9, and 12 animals when compared with day 1 animals. Protein level with $\log_2$FC > 0.6 or $\log_2$FC < −0.6 (FC, fold change) with $-\log_{10}(P$ value) > 1.3 is defined as significantly up-regulated (deep red) and down-regulated (deep blue), respectively. Twenty-three candidate genes selected for screening are labeled with yellow and green. The green dot indicates TMC-1.

and fig. S3A). These results further confirmed that we can specifically label and isolate neuronal proteins at different ages by expressing free TurboID in neurons.

We were able to identify about 1700 to 1800 proteins in each neuron-labeled sample across different ages, and these proteins are localized to different cellular organelles and cellular compartments (Fig. 1G, fig. S3B, and tables S3 and S4). We then compared the levels of each protein at different ages with those in the adult day 1 animals and found that there are age-dependent changes in proteomic profiles (Fig. 1, H to K, fig. S3C, and tables S3 and S4). Among proteins with age-dependent changes, we found that proteins associated with the translational machinery, such as ribosomal proteins, are markedly down-regulated during aging (fig. S3, D to F), which is consistent with previous findings that the overall level of protein synthesis is reduced with age in both vertebrates and invertebrates (*29*, *30*). Unexpectedly, we found that some proteins involved in the regulation of vesicle transportation and release are significantly up-regulated (fig. S3, D to F), suggesting that the activation of vesicle-associated functions may be involved in neuronal aging. To further evaluate the results from proteomics, we selected nine proteins with age-dependent expression increase and examined the expression of their functional translational reporters during aging. Consistent with the proteomic studies, all of these proteins displayed similar age-dependent increases in expression (fig. S4).

TMC-1 plays an anti-aging function in PVD, PLM, and ALM neurons

As the overall translational machinery is down-regulated, we were particularly interested in the functions of the proteins that are up-regulated with age and selected 23 conserved proteins for further examination (fig. S5, A to E). To test their functions during neuronal aging, we chose the sensory PVD, ALM, and PLM neurons as models. These neurons have different functions, exhibit distinct morphologies, and are generated from distinct lineages (*31*). The aging phenotypes of these neurons are well characterized: PLM neuron processes exhibit wavy and acute bends (*28*); PVD displayed bead structures along neuronal processes that are enriched with autophagosomes and fragmented microtubules (*27*, *32*), which is reminiscent of descriptions of mammalian neurons in neurodegenerative disease models (*33*, *34*); and ALM neurons develop a posterior process in aged animals that is associated with ALM functional decline during aging (Fig. 2A) (*28*, *32*). We quantified the percentage of animals with aging-associated phenotypes and found that the most rapid increase in penetrance of these phenotypes occurred between adult days 4 to 6 (Fig. 2B). To test the functions of the 23 proteins selected, we generated transgenes that overexpressed each of them under a pan-neuronal promoter and examined how these transgenes affected the aging-associated phenotypes of PVD, ALM, and PLM neurons in day 1, 4, and 6 adults (Fig. 2C). We found that the development of PVD, ALM, and PLM neurons appeared to be normal with all transgenes examined. For 20 of these transgenes, we observed changes in aging-associated phenotypes in at least one of the three types of neurons examined, suggesting that many of these proteins up-regulated with age play important roles during neuronal aging (Fig. 2, D to H). We found that the function of a protein in neuronal aging could differ based on neuronal type. For example, *klc-2*, the *C. elegans* homolog of kinesin light chain, has a pro-aging function in PVD neurons but an anti-aging role in ALM neurons (Fig. 2, D to F). Similarly, *strl-1*, the *C. elegans* homolog of steroidogenic acute regulatory protein, can protect against aging-associated degeneration in PLM neurons but promote ALM aging phenotypes (Fig. 2, D to F). These results suggest that different neurons may use distinct molecular mechanisms during aging. Among these 23 proteins tested, we found that *tmc-1*/Tmc had anti-aging functions in all three types of neurons (Fig. 2, D to H) and decided to further investigate the function of *tmc-1* in neuronal aging.

tmc-1 encodes a *C. elegans* homolog of Tmc channels and is a functional homolog of mammalian Tmc1, Tmc2, and Tmc3 (fig. S6, A to C) (*35*–*37*). We first generated a functional TMC-1 translational reporter and confirmed that aging up-regulated TMC1 expression in many neurons (fig. S4). Next, to further analyze *tmc-1* functions in neuronal aging, we focused our studies on PVD neurons, which are stretch-sensing mechanosensors that govern harsh touch response and display robust aging-associated neurodegeneration phenotypes (Fig. 2B) (*27*). Consistent with its anti-aging role, we found that loss of function of *tmc-1* caused early-onset aging-associated PVD degeneration, while overexpression of *tmc-1* delayed the onset of PVD degeneration (Fig. 3, A and B). To further confirm the function of *tmc-1* in neuronal aging, we examined the PVD-mediated harsh touch response, a function governed by PVD neurons, in *tmc-1* loss-of-function *(lf)* and overexpression (*OE*) strains. To exclude the potential background response from gentle touch neurons, we examined the phenotypes under the *mec-4* mutant background, which abolished the function of all gentle touch neurons (*27*, *38*). As shown in Fig. 3C, consistent with their PVD neuronal morphological changes, *tmc-1* loss-of-function and overexpression animals exhibited the same early-onset and late-onset aging-associated functional decline, respectively, when compared with control animals. Moreover, expression of *tmc-1* in all neurons fully rescued *tmc-1(lf)* phenotypes, supporting the conclusion that *tmc-1* functions in neurons and regulates aging-associated PVD degeneration (Fig. 3D). We found that expression of the mouse Tmc1 was able to rescue *tmc-1(lf)* phenotypes, suggesting that *tmc-1* may play a conserved role during neuronal aging (Fig. 3E). In addition, we noticed that even with early-onset neuronal aging, *tmc-1(lf)* animals appear to have slightly longer life spans when compared to wild-type animals (fig. S7A). In contrast, *tmc-1(OE)* animals display late-onset neuronal aging but have relatively shorter life spans than wild-type animals (fig. S7A). These results suggest that the function of *tmc-1* in neuronal aging and overall animal aging are likely different.

TMC-1 regulates aging-associated neurodegeneration through GABA

Having identified a protective role of *tmc-1*, we further investigated the molecular mechanisms underlying *tmc-1* protection during neuronal aging. Recent data show that both *C. elegans tmc-1* and mouse Tmc1 can mediate Na^+-leak currents to regulate membrane potential and increase vesicle release in muscles and neurons (*9*, *35*). As our proteomic data show that many proteins associated with vesicle release are up-regulated (fig. S3, D to F), we tested whether *tmc-1* regulated neuronal aging through control of vesicle release. There are two major types of vesicles in neurons: dense-core vesicles (DCVs) and small clear synaptic vesicles (SCVs; Fig. 4A) (*39*, *40*). We examined the effects of loss of function of *unc-31*/CADPS and *unc-13*/UNC13, two essential molecules for the

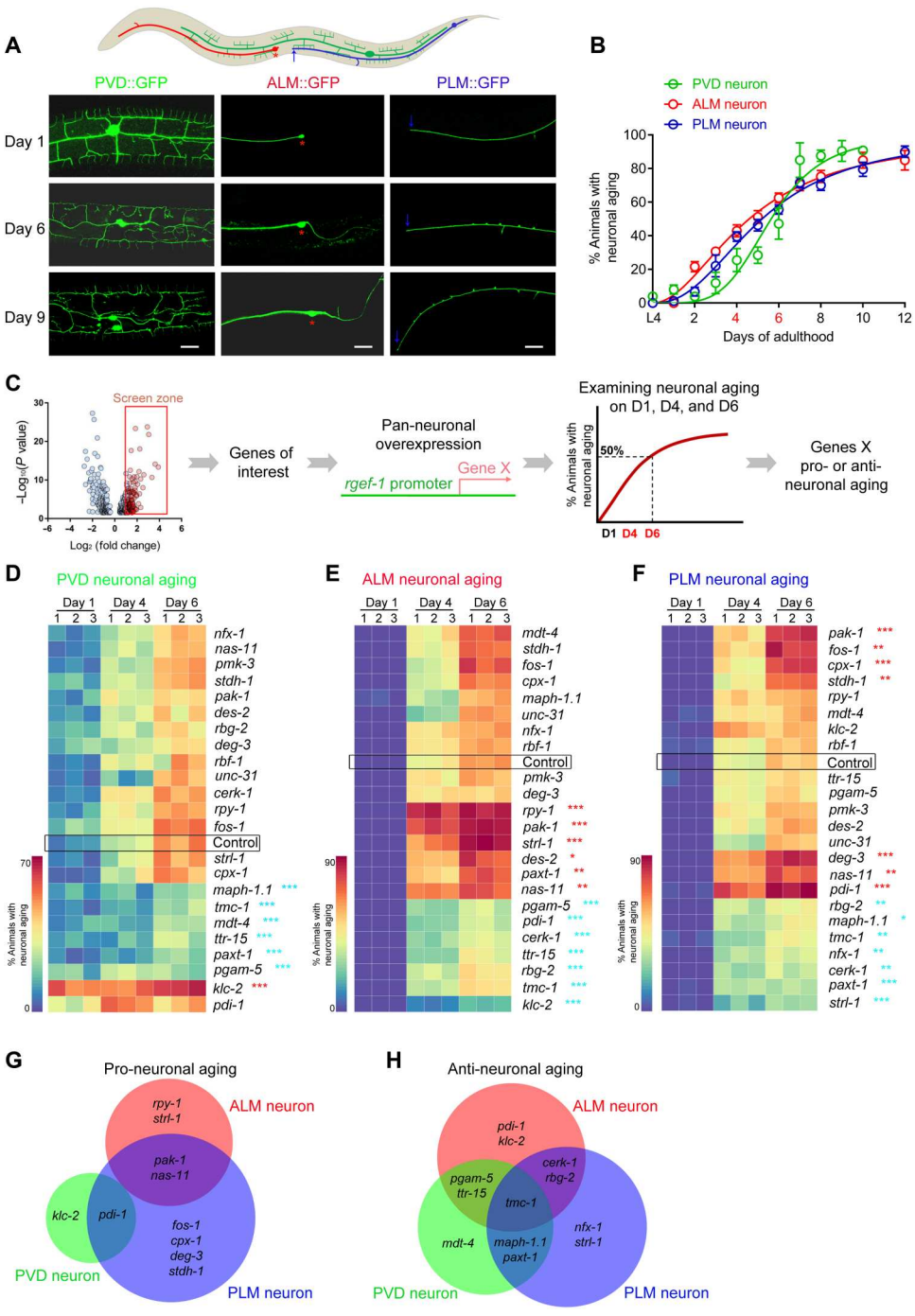

Fig. 2. Use of PVD, ALM, and PLM neurons as models to identify proteins involved in neuronal aging. (**A**) PVD, ALM, and PLM neurons display aging-associated degeneration and morphological changes. The top panel shows the schematic diagram of PVD, ALM, and PLM neurons that were labeled with green, red, and blue colors, respectively. The bottom panel shows the representative images of neurons during aging. PVD neurons were examined using *wdIs51*[*F49H12.4*::*GFP*]. ALM and PLM were visualized using *zdIs5*[*Pmec-4*::*GFP*]. The red asterisks indicate the ALM cell body. The blue arrows indicate the PLM axon terminal. Scale bars, 20 μm. (**B**) Quantification of percentage of animals with aging phenotypes. For each experiment, the percentage was calculated by the number of animals having degeneration phenotypes divided by the total number of animals observed. (**C**) Workflow for examining candidate genes. Proteins of interest are those with higher expression in day 6, 9, and 12 adults when compared with day 1 animals. Phenotypes were examined in day 1, 4, and 6 adults. (**D** to **F**) Quantification of percentage of animals with aging-associated phenotypes in PVD (D), ALM (E), and PLM (F) neurons. Results are shown in heatmaps representing three biological replicates. The names of genes tested are listed on the right side, and their mammalian homologs are listed in fig. S5E. Genes were overexpressed in the nervous system driven by a pan-neuronal promoter P*rgef-1*. The black boxes highlight the control group. Student's *t* test analysis, significant difference between control (day 6) and a specific gene overexpression group (day 6), $*P < 0.05$, $**P < 0.01$, and $***P < 0.001$. Nonsignificant comparisons are not indicated in the figure. (**G** and **H**) Summary of genes that have pro-aging (G) and anti-aging (H) functions in PVD, ALM, and PLM neurons.

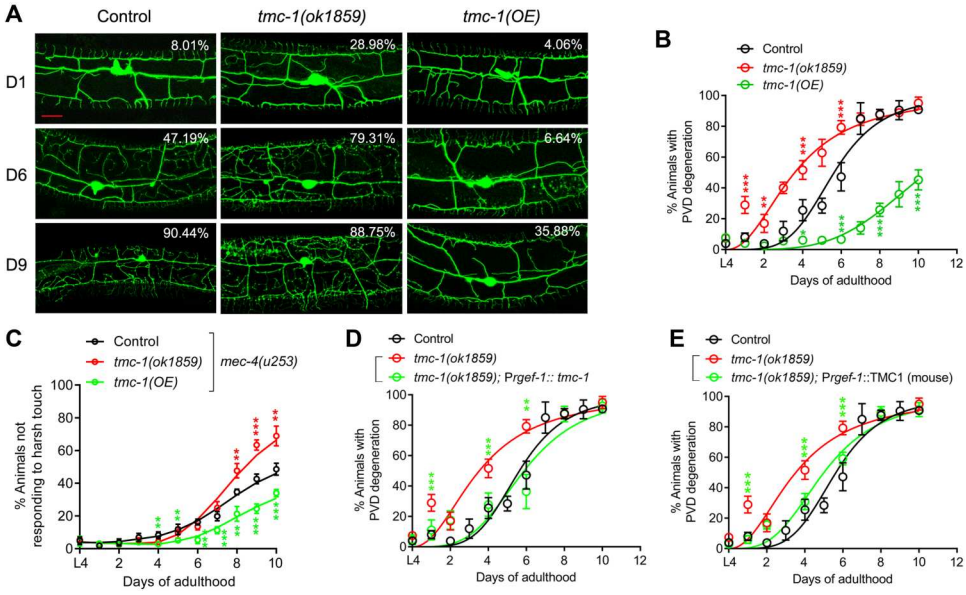

Fig. 3. TMC-1 protects neurons from aging. (**A** and **B**) *tmc-1(ok1859, null allele, lf)* and *tmc-1* overexpression (OE, *yadIs137*) caused early- and late-onset aging-associated PVD neurodegeneration, respectively. (A) Representative confocal images of PVD neurons in young and aged animals. Scale bar, 20 μm. (B) Quantification of percentage of animals with aging phenotypes. Student's *t* test, *tmc-1*(ok1859) versus control: ** (red) $P < 0.01$, *** (red) $P < 0.001$; *tmc-1*(OE) versus control: * (green) $P < 0.05$, *** (green) $P < 0.001$. Nonsignificant comparisons are not indicated in the figure. (**C**) Use of harsh touch response to analyze PVD functions. Student's *t* test, *tmc-1*(ok1859) versus control: ** (red) $P < 0.01$, *** (red) $P < 0.001$; *tmc-1*(OE) versus control: * (green) $P < 0.01$, *** (green) $P < 0.001$. Nonsignificant comparisons are not indicated in the figure. (**D**) *tmc-1* functions in neurons to regulate aging-associated PVD neurodegeneration. Neuronal-specific rescue was performed by the expression of *tmc-1* cDNA using the pan-neuronal P*rgef-1* promoter. Significant difference between *tmc-1(ok1859)* and *tmc-1(ok1859)* rescue groups, Student's *t* test, $^{**}P < 0.01$, $^{***}P < 0.001$. Nonsignificant comparisons are not indicated in the figure. (**E**) Expression of mouse Tmc1 can rescue *tmc-1(lf)* phenotypes. Significant difference between *tmc-1(ok1859)* and *tmc-1(ok1859)* rescue groups, Student's *t* test, $^{***}P < 0.001$. Nonsignificant comparisons are not indicated in the figure.

release of DCVs and SCVs, respectively (*40*), on aging-associated PVD degeneration in *tmc-1(OE)* animals. As shown in Fig. 4 (B and C), loss of function of *unc-13* but not *unc-31* completely suppresses the neuroprotective function of *tmc-1* overexpression. Similar to *tmc-1(lf)* animals, *unc-13(lf)* animals experience early-onset PVD degeneration, and *unc-13(lf);tmc-1(lf)* double mutants showed similar degrees of PVD degeneration when compared with *unc-13(lf)* single mutants (Fig. 4D). These results support the conclusion that *tmc-1* regulates aging-associated PVD neurodegeneration by modulating the release of SCVs. To further confirm this conclusion, we examined the function of other molecules involved in the release of SCVs, including *unc-18*/STXBP1, *snb-1*/VAMP2, *unc-64*/STX1A/B, and *rab-3*/RAB3A (Fig. 4A) (*41*–*43*). Results showed that loss of function of any of them could attenuate the late-onset PVD degeneration mediated by *tmc-1* overexpression (Fig. 4, E to H). We found that although loss of function of *unc-18* caused strong early-onset PVD degeneration similar to that in *unc-13(lf)* animals, loss of function of *snb-1*, *rab-3*, or *unc-64* had little to no effect on aging-associated PVD degeneration (Fig. 4, E to H), suggesting that different proteins involved in the release of SCVs may contribute differently to neuronal aging. In summary, these data show that *tmc-1* protects neurons from aging-associated degeneration through regulation of SCV release. While *tmc-1* is known to mediate Na^+-leak currents to regulate membrane potential (*35*), the function of *tmc-1* is likely not only through increase of neuronal activity, as enhancing neuronal activity by loss of function in *slo-1*/potassium channel or gain of function in *egl-19*/voltage-gated calcium channel (*44*, *45*) did not cause the same anti-aging effect as in *tmc-1(OE)* animals (Fig. 4I).

In neurons, SCVs mainly mediate the release of neurotransmitters, including glutamate (Glu), acetylcholine (Ach), serotonin [5-hydroxytryptamine (5-HT)], dopamine (DA), tyramine (TA), octopamine (OA), and GABA (Fig. 5A) (*46*). To test which neurotransmitters may play a role in the neuroprotective function of TMC-1, we examined the effects of loss of each neurotransmitter on *tmc-1(OE)* phenotypes by mutating key synthetic enzymes. As shown in Fig. 5C, abolishment of GABA by mutating *unc-25*, the only glutamic acid decarboxylase (GAD) for GABA synthesis in *C. elegans* (*47*), completely suppressed the neuroprotection function of *tmc-1*, while the absence of other neurotransmitters did not significantly affect *tmc-1(OE)* phenotypes (Fig. 5, B and C). To further confirm the role of GABA in TMC-1–mediated neuroprotection, we examined the effect of loss of function in *unc-30/PITX2*, an essential transcriptional factor for the fate determination of GABAergic neurons (*48*), and found that *unc-30(lf)* mutants also fully suppress the late-onset PVD neurodegeneration phenotypes in *tmc-1(OE)* animals (Fig. 5D). Moreover, supplement of animals with exogenous GABA fully suppressed the early-onset PVD degeneration in *tmc-1(lf)* animals (fig. S8A). These results demonstrate that the neuroprotective function of TMC-1 occurs by regulating GABA release and suggest that TMC-1 likely functions in GABAergic neurons to prevent aging-associated PVD neurodegeneration in a non–cell-autonomous manner. To test this hypothesis, we examined the ability of *tmc-1* expression in GABAergic, cholinergic, and serotonergic neurons to rescue *tmc-1(lf)* phenotypes and found that

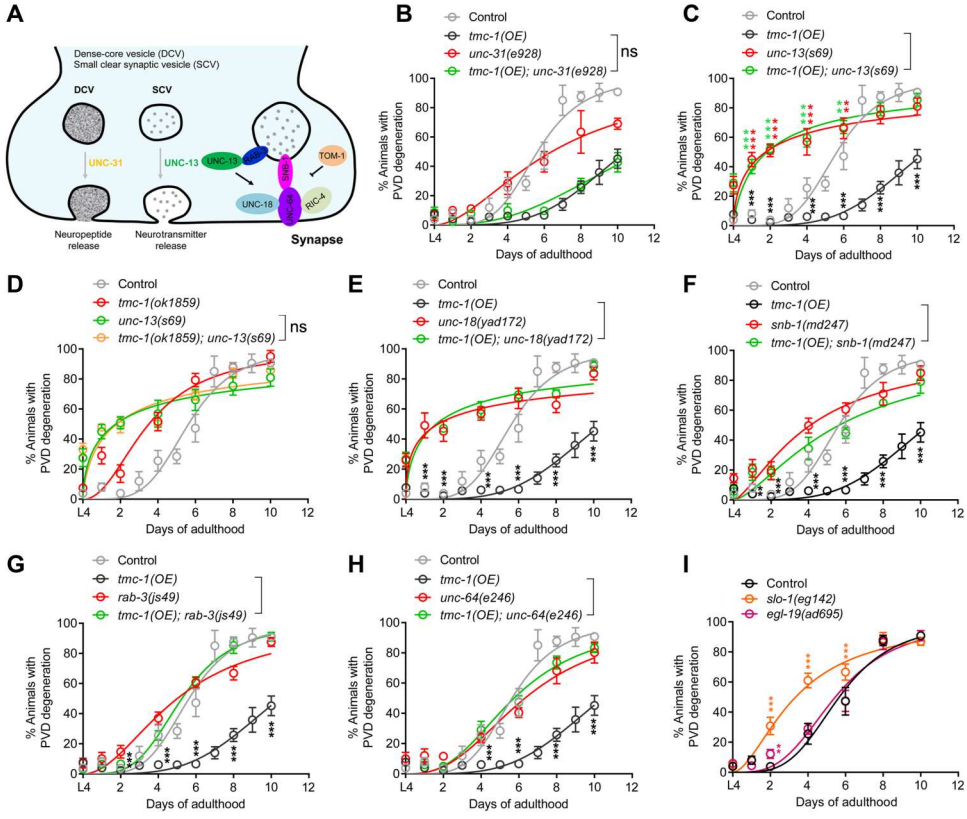

Fig. 4. TMC-1 regulates neuronal aging through control of synaptic vesicle release. (**A**) Schematic of DCV and SCV release in neurons. (**B**) Quantification of percentage of animals with PVD neurodegeneration in control, *tmc-1(OE,yadls137)*, *unc-31 (e928)*, and *tmc-1(OE,yadls137);unc-31(e928)* strains. Student's *t* test showed no differences between *tmc-1(OE,yadls137)* and *tmc-1(OE,yadls137);unc-31(e928)* at any time point. Nonsignificant comparisons are not indicated in the figure. (**C**) Quantification of percentage of animals with PVD neurodegeneration in control, *tmc-1(OE,yadls137)*, *unc-13 (s69)*, and *tmc-1(OE,yadls137);unc-13(s69)* strains. Significant difference between *tmc-1(OE,yadls137)* and *tmc-1(OE,yadls137);unc-13(s69)*, Student's *t* test analysis for each day, *** (black) $P < 0.001$. Significant difference between control, *unc-13(s69)*, and *tmc-1(OE,yadls137);unc-13(s69)*, one way analysis of variance (ANOVA) analysis for each day, *unc-13(s69)* versus control: ** (red) $P < 0.01$, *** (red) $P < 0.001$; *tmc-1(OE,yadls137);unc-13(s69)* versus control: ** (green) $P < 0.01$, *** (green) $P < 0.001$. Nonsignificant comparisons are not indicated in the figure. (**D**) Quantifications of percentage of animals with PVD neurodegeneration in control, *tmc-1(ok1859)*, *unc-13(s69)*, and *tmc-1(ok1859);unc-13(s69)* strains. Student's *t* test showed no differences between *tmc-1(ok1859);unc-13(s69)* and *unc-13(s69)* at any time point (ns, no significant difference). (**E** to **H**) Quantification of percentage of animals with PVD neurodegeneration in mutants of vesicle release–associated genes, *unc-18(yad172)*, *snb-1(md247)*, *rab-3(js49)*, and *unc-64(e246)*, and these mutations in the *tmc-1(OE, yadls137)* background. Significant difference between *unc-18(yad172)* and *tmc-1(OE,yadls137);unc-18(yad172)* (E), *snb-1(md247)* and *tmc-1(OE,yadls137);snb-1(md247)* (F), *rab-3(js49)* and *tmc-1(OE,yadls137); rab-3(js49)* (G), and *unc-64(e246)* and *tmc-1(OE,yadls137);unc-64(e246)* (H). Student's *t* test analysis for each day, **$P < 0.01$, ***$P < 0.001$. Nonsignificant comparisons are not indicated in the figure. (**I**) Quantification of percentage of animals with PVD neurodegeneration in control, *slo-1(eg142,lf)*, and *egl-19(ad695, gf)* animals. Significant difference between control and *slo-1(eg142)*, Student's *t* test analysis for each day, ***$P < 0.001$. Nonsignificant comparisons are not indicated in the figure.

GABAergic expression of *tmc-1* can fully rescue early-onset PVD neurodegeneration phenotypes in *tmc-1(lf)* animals (Fig. 5E), whereas cholinergic and serotonergic expressions did not affect *tmc-1(lf)* phenotypes (Fig. 5, F and G). Furthermore, expression of *tmc-1* only in GABAergic neurons also causes late-onset PVD neurodegeneration similar to that of pan-neuronal *tmc-1* overexpression, whereas overexpressing *tmc-1* in cholinergic and serotonergic neurons did not affect aging-associated PVD degeneration (Fig. 5H). In conclusion, our results show that TMC-1 functions in GABAergic neurons and by regulating GABA release to control aging-associated PVD neurodegeneration. Because PVD neurons do not have any inputs from GABAergic neurons (*31*), our results also suggest that extrasynaptic GABA plays a key role in aging-associated PVD neurodegeneration.

Metabotropic $GABA_B$ receptor GBB-1 mediates the neuroprotective function of TMC-1–GABA signals

Although they do not receive any direct inputs from GABAergic neurons, PVD neurons express both ionotropic $GABA_A$ and metabotropic $GABA_B$ receptors (*25*, *26*). To test whether these GABA receptors are involved in aging-associated PVD neurodegeneration, we treated *tmc-1*(OE) animals with bicuculline and gabazine, two $GABA_A$ receptor antagonists, and saclofen, a $GABA_B$ receptor antagonist, respectively (Fig. 6A) (*14*, *22*, *49*). As shown in Fig. 6B, saclofen treatments suppress late-onset PVD neurodegeneration phenotypes in *tmc-1(OE)* animals, while bicuculline and gabazine had little to no effects on PVD degeneration in *tmc-1(OE)* animals, supporting the conclusion that metabotropic $GABA_B$ but not ionotropic $GABA_A$ receptors are required for the neuroprotective function of TMC-1. This conclusion was further supported by

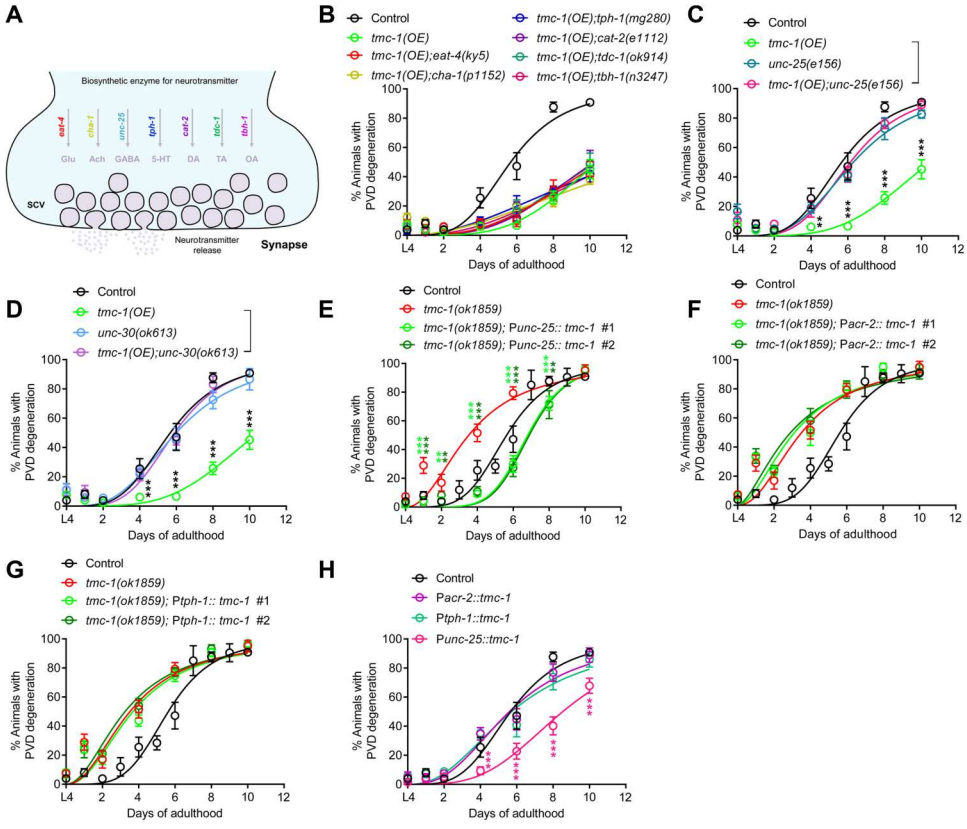

Fig. 5. GABA is required for the neuroprotective function of TMC-1. (**A**) Schematic of neurotransmitters and their key biosynthetic enzymes in synapses. (**B** and **C**) Quantification of percentage of animals with PVD neurodegeneration in control, *tmc-1(OE,yadls137)*, and *tmc-1(OE,yadls137)* in different mutant backgrounds. Significant difference between *tmc-1(OE,yadls137)* and *tmc-1(OE,yadls137);unc-25*, Student's *t* test analysis for each day, $^{**}P < 0.01$, $^{***}P < 0.001$. Nonsignificant comparisons are not indicated in the figure. (**D**) Quantification of percentage of animals with PVD neurodegeneration in control, *tmc-1(OE,yadls137)*, and *tmc-1(OE,yadls137);unc-30(ok613)* animals. Significant difference between *tmc-1(OE,yadls137)* and *tmc-1(OE,yadls137);unc-30(ok613)*, Student's *t* test analysis for each day, $^{***}P < 0.001$. (**E** to **G**) *tmc-1* functions in GABAergic neurons to regulate PVD neurodegeneration. GABAergic-specific rescue was performed by expression of *tmc-1* cDNA driven by the GABAergic-specific promoter P*unc-25*, cholinergic-specific promoter P*acr-2*, and serotonergic-specific promoter P*tph-1*, respectively. Significant difference between *tmc-1(ok1859)* and *tmc-1(ok1859)* GABAergic rescue groups, Student's *t* test analysis for each day, $^{**}P < 0.01$, $^{***}P < 0.001$. Nonsignificant comparisons are not indicated in the figure. (**H**) Quantification of percentage of animals with PVD neurodegeneration in control, *tmc-1* GABAergic (P*unc-25*), cholinergic (P*acr-2*), and serotonergic (P*tph-1*) overexpression transgenes. Significant difference between control and *tmc-1* GABAergic overexpression groups, Student's *t* test analysis for each day, $^{***}P < 0.001$. Nonsignificant comparisons are not indicated in the figure.

results from examination of animals treated with the $GABA_B$ agonist baclofen (*14*, *22*), in which we found that activation of $GABA_B$ receptors delayed the onset of PVD degeneration in control animals (Fig. 6C) and fully suppressed the early-onset PVD degeneration in *tmc-1(lf)* animals (fig. S8B). Together, these results demonstrate that extrasynaptic GABA functions on metabotropic $GABA_B$ receptors to transduce the neuronal protective signals from GABAergic TMC-1 expression.

C. elegans express two metabotropic $GABA_B$ receptors, *gbb-1* and *gbb-2*, homologs of mammalian GABBR1 and GABBR2 (*50*), and they are broadly expressed in almost 90% of neurons including PVD neurons (fig. S7C) (*26*). To address which $GABA_B$ receptors mediate the extrasynaptic GABA signals triggered by GABAergic TMC-1 expression, we examined the effects of mutating *gbb-1(yad225)* and *gbb-2(yad227)* in *tmc-1(OE)* animals (fig. S7B). Our results showed that loss of function of *gbb-1*, but not *gbb-2*, attenuated the late-onset PVD degeneration in *tmc-1(OE)* animals, and *gbb-1* functions cell autonomously to mediate the neuroprotective function of *tmc-1(OE)* (Fig. 6, D and E). These data supported the conclusion that GABAergic *tmc-1* expression can promote the release of extrasynaptic GABA, which then activates the $GABA_B$ receptor GBB-1 in PVD neuron to protect PVD neurons from degeneration during aging.

TMC-1–GABA signals protect neurons by inhibiting the PKC pathway

Metabotropic $GABA_B$ receptors are G protein–coupled receptors, which elicit slow and sustained activity by triggering signal transduction pathways via Gi/o proteins (Fig. 7A) (*22*). We therefore tested whether Gi/o proteins were required for *tmc-1(OE)* phenotypes and found that expression of pertussis toxin (PTX), a specific inhibitor of Gi/o activation (*51*, *52*), in PVD neurons completely suppressed *tmc-1(OE)* phenotypes (Fig. 7B), illustrating the cell-autonomous role of G proteins in *tmc-1(OE)*–mediated neuroprotection. Moreover, loss of function in *goa-1*, an ortholog of human GNAO1 (G protein subunit alpha o1), attenuated late-onset PVD degeneration phenotypes in *tmc-1(OE)* animals (Fig. 7C). These results support the conclusion that the metabotropic $GABA_B$

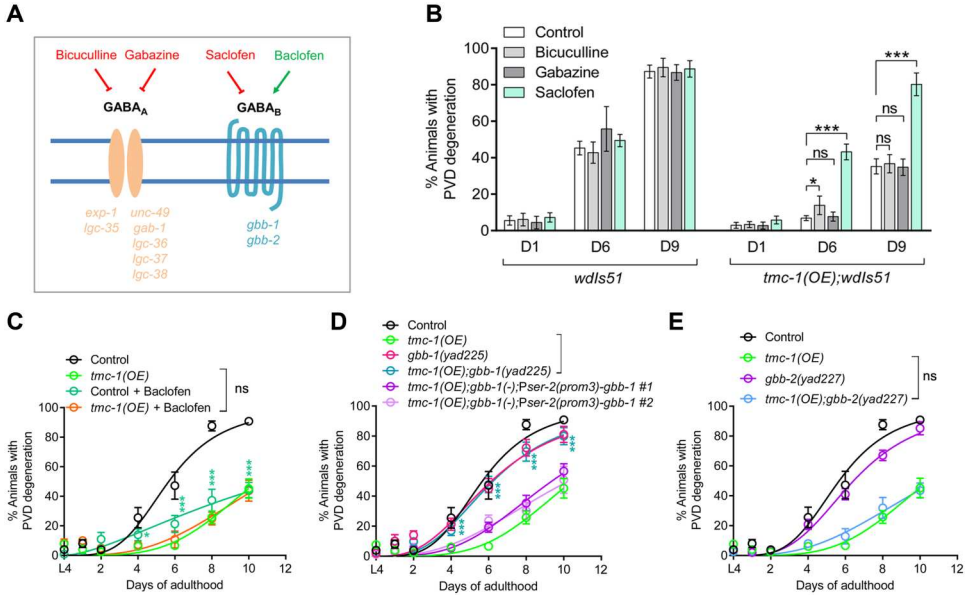

Fig. 6. The neuroprotective function of TMC-1–GABA signals acts through the $GABA_B$ receptors. (**A**) Schematic of antagonists and agonists of $GABA_A$ and $GABA_B$ receptors. (**B**) Quantification of the percentage of animals with PVD neurodegeneration in control(*wdIs51*) and *tmc-1(OE,yadIs137);wdIs51* animals treated with different antagonists for $GABA_A$ or $GABA_B$ receptor. Student's *t* test analysis, $*P < 0.05$, $***P < 0.001$. (**C**) Quantification of percentage of animals with PVD neurodegeneration in control and *tmc-1(OE,yadIs137)* animals treated with or without $GABA_B$ receptor agonist. Significant difference between control animals treated with and without baclofen, Student's *t* test analysis for each day, $*P < 0.05$, $***P < 0.001$. Statistical analyses of *tmc-1(OE, yadIs137)* animals with and without baclofen show no differences. Nonsignificant comparisons are not indicated in the figure. (**D**) Quantification of percentage of animals with PVD neurodegeneration in control, *tmc-1(OE,yadIs137)*, *gbb-1 (yad225)*, *tmc-1(OE,yadIs137);gbb-1(yad225)*, and PVD-specific rescue of *gbb-1* in *tmc-1(OE,yadIs137);gbb-1(yad225)* background. Significant difference between *tmc-1(OE, yadIs137)* and *tmc-1(OE,yadIs137);gbb-1(yad225)*, Student's *t* test analysis for each day, $***P < 0.001$. (**E**) Quantification of percentage of animals with PVD neurodegeneration in control, *tmc-1(OE,yadIs137)*, *gbb-2 (yad227)*, and *tmc-1(OE,yadIs137);gbb-1(yad227)* strains. Analyses between *tmc-1(OE, yadIs137)* and *tmc-1(OE,yadIs137);gbb-2(yad227)* show no significant differences, Student's *t* test analysis for each day. Nonsignificant comparisons are not indicated in the figure.

receptors function as G protein–coupled receptors via Go proteins to mediate TMC-1 signaling in regulation of aging-associated PVD degeneration. As activation of Go proteins can cause the suppression of adenosine 3′,5′-monophosphate (cAMP), guanosine 3′,5′-monophosphate (cGMP), and phospholipase Cβ (PLCβ) signals in *C. elegans* (Fig. 7A) (*53*, *54*), we individually tested the functional significance of these three pathways in *tmc-1(OE)*–mediated neuroprotection. To activate the cAMP-PKA pathway, we examined the effect of loss of function in *pde-4*/phosphodiesterase 4B and *kin-2*/cAMP-dependent protein kinase type Iα regulatory subunit, negative regulators for cAMP synthesis and PKA activation, respectively, on *tmc-1(OE)* phenotypes, and found that neither of them affected the *tmc-1(OE)*–mediated neuroprotection (Fig. 7, D and E). We next examined whether activation of the cGMP-PKG pathway by a gain-of-function mutation of *egl-4*/PKG could suppress *tmc-1(OE)* phenotypes and found that *egl-4(gf)* did not affect *tmc-1(OE)* phenotypes (Fig. 7F). Last, we showed that *egl-8*/PLCβ*(lf)* mutants exhibited the same degree of late-onset PVD neurodegeneration as that in *tmc-1(OE)* animals, and mutating *egl-8* in the *tmc-1(OE)* background did not further enhance the phenotypes when compared with *egl-8(lf)* or *tmc-1(OE)* animals (Fig. 7G). These results support the conclusion that *tmc-1(OE)*–mediated neuroprotection happens through regulation of the *egl-8*/PLCβ but not cAMP-PKA or cGMP-PKG pathways. As *goa-1*/$G\alpha_o$ inhibits *egl-8*/PLCβ through *egl-30*/$G\alpha_q$ (Fig. 8A) (*53*, *55*), we further examined the function of *egl-30*/$G\alpha_q$ in aging-associated PVD degeneration and found that *egl-30(lf)* animals exhibited similar neuroprotection phenotypes as those in *egl-8(lf)* and *tmc-1(OE)* animals, and that *tmc-1(OE); egl-30(lf)* did not enhance neuroprotection (Fig. 8B). In summary, these data demonstrate that TMC-1–GABA functions through GOA-1 to inhibit PLCβ activity and delay the onset of aging-associated PVD neurodegeneration.

PLCβ activates two main downstream pathways: the release of intracellular calcium by activating inositol 1,4,5-triphosphate (IP_3) receptors (*56*) and the activation of PKC through diacylglycerol (DAG; Fig. 8A) (*55*, *57*). We first examined whether expression of IP_3 super-sponge, a genetic inhibitor of IP_3 receptor (*56*, *58*), in PVD neurons could protect PVD neurons from aging-associated degeneration (Fig. 8C), and found that in contrast to *tmc-1(OE)*, inhibition of IP_3 receptor caused early-onset, but not late-onset, PVD neurodegeneration (Fig. 8D). Next, we tested the function of the DAG-PKC pathway in *tmc-1(OE)*–mediated neuroprotection by mutating *dgk-1*/DAG kinase, a negative regulator of DAG synthesis (*59*, *60*), and found that *dgk-1(lf)* completely suppressed the late-onset PVD degeneration phenotypes in *tmc-1(OE)* animals (Fig. 8E). Furthermore, loss of function of *pkc-1*/PKC exhibited the same degree of late-onset PVD degeneration phenotypes as that in *tmc-1(OE)* animals, and *pkc-1(lf);tmc-1(OE)* did not further delay the onset of PVD degeneration when compared with *tmc-1(OE)* or *pkc-1(lf)* (Fig. 8F). In addition, we found that expression of a constitutively active form of PKC-1(A160E) (*61*) in PVD neurons suppressed *tmc-1(OE)*–mediated neuroprotection (Fig. 8F), and *pkc-1(lf)* fully suppressed the early-onset PVD degeneration in *tmc-1(lf)* animals (fig. S9). Our results also showed that

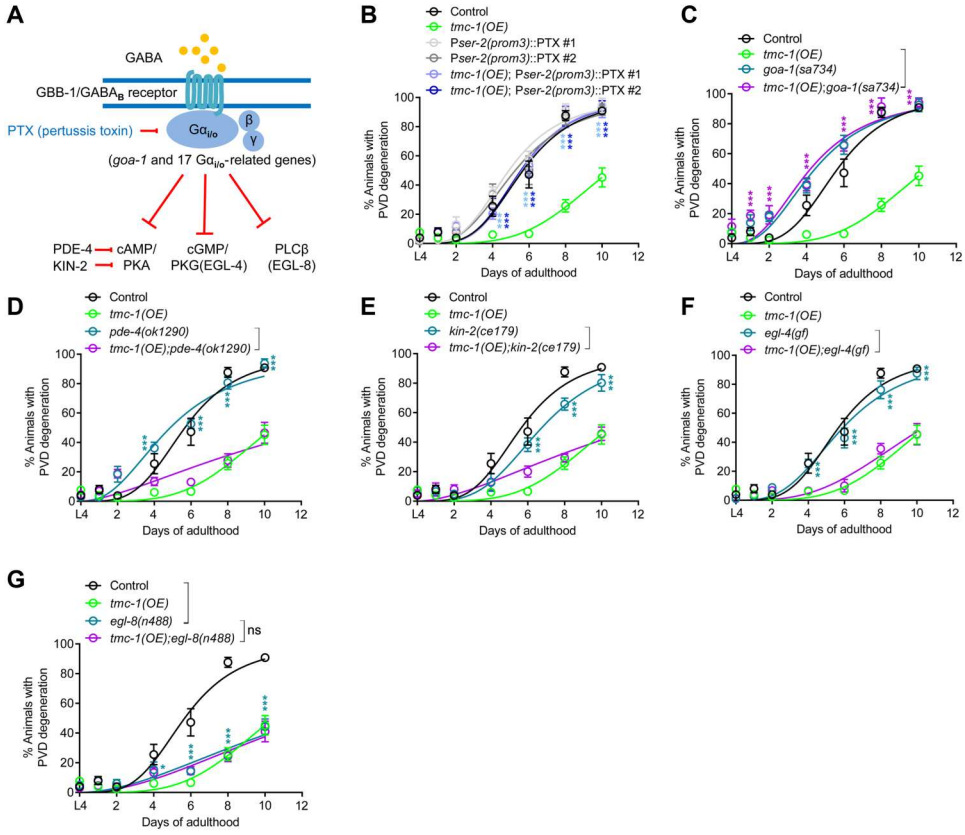

Fig. 7. The neuroprotective function of TMC-1–GABA signals acts by inhibiting the PLCβ. (**A**) Schematic of signals regulated by Gi/o proteins. (**B**) Quantification of the percentage of animals with PVD neurodegeneration in control, *tmc-1(OE,yadls137)*, and PVD-specific expression of PTX in *tmc-1(OE,yadls137)* background. Significant difference between the *tmc-1(OE, yadls137)* and PVD-specific expression of PTX in *tmc-1(OE,yadls137)* groups, Student's *t* test analysis for each day, ***$P < 0.001$. (**C**) Quantification of percentage of animals with PVD neurodegeneration in control, *tmc-1(OE,yadls137)*, *goa-1(sa734)*, and *tmc-1(OE,yadls137);goa-1(sa734)* strains. Significant difference between *tmc-1(OE, yadls137)* and *tmc-1(OE,yadls137);goa-1(sa734)*, Student's *t* test analysis for each day, ***$P < 0.001$. (**D** to **G**) Identification of downstream signals of Gi/o that mediate TMC-1 and GABA neuron-protective functions. *Pde-4(ok1290)* and *kin-2(ce179)* are two mutants with increased PKA activity. *Egl-4(ad450)* is a gain-of-function mutant with increased PKG activity. *Egl-8(n488)* is a loss of function of mutant *egl-8*/PLCβ. Student's *t* test for each day, *pde-4(ok1290)* versus *tmc-1(OE); pde-4(ok1290)*: ***$P < 0.001$ (D); *kin-2(ce179)* versus *tmc-1(OE); kin-2(ce179)*: ***$P < 0.001$ (E); *egl-4(ad450)* versus *tmc-1(OE); egl-4(ad450)*: ***$P < 0.001$ (F); *egl-8(n488)* versus *tmc-1(OE); egl-8(n488)*: no significant difference (F). Significant difference between control and *egl-8(n488)*, Student's *t* test analysis for each day, *$P < 0.05$, ***$P < 0.001$ (G). Nonsignificant comparisons are not indicated in the figure.

PKC exhibited higher expression and activation levels in aged animals when compared with young ones, and *tmc-1(OE)* suppressed this age-dependent increase of PKC expression and activation (fig. S10, A to C), supporting the conclusion that the function of TMC-1–GABA signals is by regulating PKC-1 expression and activation during aging. Together, we show that extrasynaptic GABA signaling mediated by GABAergic TMC-1 expression can activate GABA$_B$ receptor/GOA-1 and inhibit the PLCβ-DAG-PKC pathway to protect neurons from degeneration during aging.

The TMC-1–GABA–PKC signaling axis regulates aging-associated declines in locomotion and axon regeneration

As *tmc-1* is broadly expressed in the nervous system and protects PVD neurons against neuronal aging, we asked whether the TMC-1–GABA–PKC signaling axis could be a more general regulator of neuronal aging. To address this question, we compared aging-associated decline of locomotion in *tmc-1(lf)* and *tmc-1*(OE) animals. *C. elegans* locomotion is a complex behavior and is controlled by many neurons including interneurons and motor neurons (Fig. 9A) (*62*), and the age-associated decline of locomotion is a consequence of neuronal aging (*63*, *64*). Consistent with previous findings, control animals displayed an age-dependent decrease in locomotion, with day 9 adults displaying only about 20 to 30% of the locomotion of day 1 animals (Fig. 9, B and C). Overexpression of *tmc-1* significantly suppressed the decline of locomotion in aged animals, and the average speed of *tmc-1*(OE) day 9 adults is more than twice that of the same-age control animals (Fig. 9, B and C). The effects observed in *tmc-1*(OE) animals are not due to an overall increase in mobility because *tmc-1*(OE) day 1 young adults exhibit similar locomotion as the same-age control animals (Fig. 9, B and C). Consistent with its anti-aging role, loss of function of *tmc-1* also led to early-onset decline of locomotion (Fig. 9, B and C). As loss of function in GABA caused locomotion defects (*47*), we examined the locomotion phenotypes of *rab-3(lf)* and *gbb-1(lf)* mutants, which have relatively normal locomotion but disrupt synaptic vesicle release and metabotropic GABA receptors, respectively. Consistent with our findings in aging-associated PVD degeneration, we found that loss of function of *rab-3* or *gbb-1* abolished

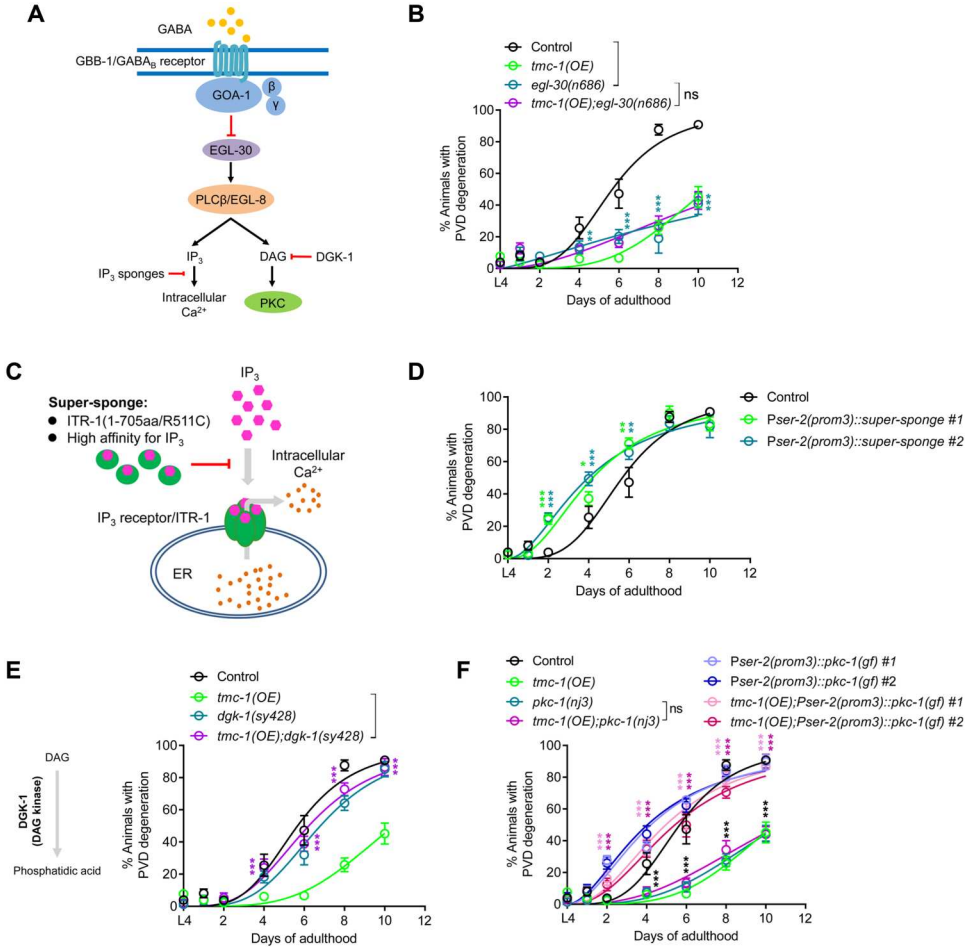

Fig. 8. The PLCβ-DAG-PKC pathway functions at the downstream of TMC-1–GABA signals to protect neurons from aging. (**A**) Schematic of the GOA-1–EGL-30–EGL-8 pathway. (**B**) Quantification of percentage of animals with PVD neurodegeneration in control, *tmc-1(OE,yadls137)*, *egl-30(n686)*, and *tmc-1(OE,yadls137);egl-30(n686)* strains. Significant difference between control and *egl-30(n686)*, Student's *t* test analysis for each day, $^{**}P < 0.01$, $^{***}P < 0.001$. (**C**) A schematic diagram shows how the inositol 1,4,5-trisphosphate (IP_3) signal is blocked by expressing IP_3 super-sponge. IP_3 diffuses to the endoplasmic reticulum (ER), where it activates the IP_3 receptor (ITR-1), resulting in the release of Ca^{2+} into the cytoplasm. IP_3 super-sponge is an N-terminal fragment (1 to 705 amino acids) of ITR-1 with a mutation (R511C) on the IP_3 binding domain. Expression of IP_3 super-sponge could competitively bind with IP_3 to interfere with the IP_3 receptor activation. (**D**) Quantification of percentage of animals with PVD neurodegeneration in control and PVD-specific expression of IP_3 super-sponge transgenes. Significant difference between control and PVD IP_3 super-sponge–expressing transgenic animals, Student's *t* test analysis for each day, $^{*}P < 0.05$, $^{**}P < 0.01$, and $^{***}P < 0.001$. (**E**) Quantification of percentage of animals with PVD neurodegeneration in control, *tmc-1(OE)*, *dgk-1(sy428)*, and *tmc-1(OE);dgk-1(sy428)* strains. Significant difference between *tmc-1(OE)* and *tmc-1(OE);dgk-1(sy428)*, Student's *t* test analysis for each day, $^{***}P < 0.001$.(**F**) Quantification of percentage of animals with PVD neurodegeneration in control, *tmc-1(OE)*, *pkc-1(nj3)*, *tmc-1(OE);pkc-1(nj3)*, and PVD-specific expression of *pkc-1(gf)* in control or *tmc-1(OE)* strains. *pkc-1(nj3)* is a null allele (W218stop). *pkc-1(gf)* is a constitutively active form of PKC-1 carrying an A160E mutation in the autoinhibitory pseudosubstrate motif (*61*). Student's *t* test for each day, control versus *pkc-1(nj3)*: *** (black) $P < 0.001$; *tmc-1(OE)* versus PVD-specific expression of *pkc-1(gf)* under the *tmc-1(OE)* background: *** (rose-red) $P < 0.001$. Significance analysis between *pkc-1(nj3) and tmc-1(OE);pkc-1(nj3)* showed no differences. Nonsignificant comparisons are not indicated in the figure.

the protective effect of *tmc-1* overexpression on aging-associated locomotion decline (Fig. 9, B and C). Similarly, activation of $GABA_B$ receptors by baclofen suppressed locomotion decline upon aging (Fig. 9, B and C). As the downstream target of the TMC-GABA signals, loss of function in *pkc-1* delayed aging-associated locomotion decline similar to that in *tmc-1(OE)* animals, and *pkc-1(lf);tmc-1(OE)* did not further delay the onset of locomotion decline when compared to *tmc-1(OE)* or *pkc-1(lf)* animals (Fig. 9, B and C). In conclusion, these data demonstrate that the TMC-1–GABA–PKC signaling axis regulates aging-associated locomotion decline.

Aging not only causes neurodegeneration and functional decline but also affects how neurons respond to injury. Recent studies showed that aged animals exhibited weaker axon regeneration after axotomy when compared to young animals (*65*, *66*). *C. elegans* PLM neurons exhibited robust aging-associated decline in axon regeneration (*65*). We therefore tested whether the TMC-1–GABA–PKC signaling axis could also regulate this aging-associated decline in PLM axon regeneration. *tmc-1(OE)* significantly improved the axon regeneration ability of day 5 animals, and this effect is due to suppression of aging-associated decline in axon regeneration rather than promoting axon regeneration because *tmc-1(OE)*

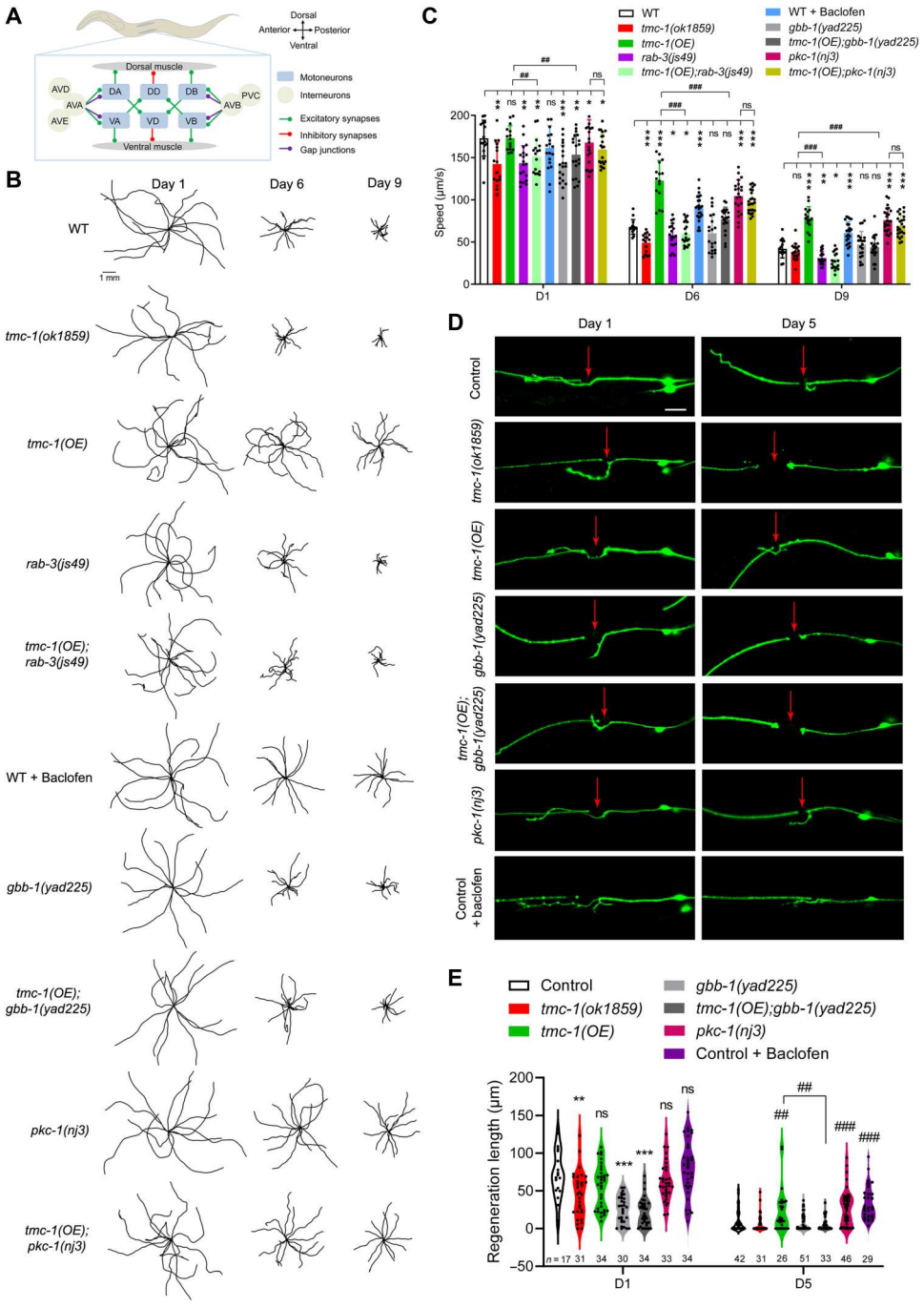

Fig. 9. The TMC-1–GABA–PKC signaling axis regulates aging-associated decline of locomotion and axon regeneration. (**A**) Schematic of the *C. elegans* locomotive neural circuit. (**B**) Representative 30-s locomotion trajectories superimposed for 12 animals of each experiment group as indicated. The starting points for each trajectory are aligned for clarity. Scale bar, 1 mm. (**C**) Quantification of the average locomotion speed of animals. Data are presented as means ± SD of at least 15 animals. One-way ANOVA, $^{*}P < 0.05$, $^{**}P < 0.01$, $^{***}P < 0.001$. Significant difference between *tmc-1(OE)* and *tmc-1(OE);rab-3(js49)*, or *tmc-1(OE);gbb-1(yad225)*, respectively, one-way ANOVA, $^{\#\#}P < 0.01$, $^{\#\#\#}P < 0.001$. (**D**) Representative confocal images of PLM axons at 24 hours after axotomy. The red arrows indicate the cutting sites. Scale bar, 20 μm. (**E**) Quantification of PLM regrowth length at 24 hours after axotomy. *n*, number of animals used for quantification. Data are presented as means ± SD. One-way ANOVA, in day 1 group, $^{**}P < 0.01$, $^{***}P < 0.001$; in day 5 group, $^{\#\#}P < 0.01$, $^{\#\#\#}P < 0.001$.

did not affect axon regeneration in day 1 animals (Fig. 9, D and E). Consistent with its anti-aging role, *tmc-1(lf)* animals have weaker axon regeneration ability even in young adults when compared with the same-age control animals (Fig. 9, D and E). To address whether the late-onset axon regeneration decline in *tmc-1(OE)* animals was through GABA signals, we further examined PLM axon regeneration in *gbb-1(lf);tmc-1(OE)* animals and found that loss of function of *gbb-1* abolished the effects of *tmc-1(OE)* (Fig. 9, D and E). We also noticed that *gbb-1(lf)* mutants had shorter regeneration length in young adults when compared with the same-age control animals, which is consistent with the anti-neuronal aging function of *gbb-1* (Fig. 9, D and E). Similar to our findings, a previous genetic screen for PLM axon regeneration revealed that abolishment of GABA synthesis by mutating *unc-30* or *unc-25* can also significantly suppress axon regeneration in day 1 animals (*67*). In additional, activation of $GABA_B$ receptors by baclofen suppressed the decline of axon regeneration in aged animals but did not affect axon regeneration in younger ones (Fig. 9, D and E). As PLM neurons do not receive any synaptic inputs from GABAergic neurons (*31*), these results further support the important anti-aging function of extrasynaptic GABA. Because *pkc-1* functions downstream of TMC-1–GABA signals to regulate aging-associated PVD neurodegeneration and locomotion decline, we further examined the function of *pkc-1* in PLM axon regeneration and showed that *pkc-1(lf)* increased the regrowth ability in day 5 animals to a level similar to *tmc-1(OE)* animals (Fig. 9, D and E). In conclusion, we show that the TMC-1–GABA–PKC signaling axis plays a critical role in regulating the aging-associated decline in axon regeneration.

Activation of the TMC-1–GABA–PKC signaling axis improves neuronal function in an Alzheimer's disease model

Previous studies suggest that aging-associated neurodegenerative diseases such as Alzheimer's disease may use similar mechanisms as those involved in neurodegeneration associated with physiological aging (*68*). Having observed the robust anti-neuronal aging and anti-aging–associated neurodegeneration function of *tmc-1*, we further tested whether expression of *tmc-1* could protect neurons in disease conditions. To do so, we used a *C. elegans* Alzheimer's disease model, which overexpresses the F3 pro-aggregation fragment of the human Tau protein in all neurons {*byIs161* [*rab-3p::F3*(*delta*)*K280*]} (*69*). Consistent with previous studies, we found that expression of this pro-aggregation fragment of the human Tau protein caused locomotive decline in *C. elegans* (Fig. 10, A and B), confirming that this model may reflect some of the neuronal features in Alzheimer's disease patients (*69*). Our results also showed that expression of this human Tau protein fragment did not affect TMC-1 expression in young or aged animals when compared with the same age control animals (fig. S11, A and B). Next, we examined the effect of overexpressing *tmc-1* and found that *tmc-1(OE)* suppressed the locomotion decline in this Alzheimer's disease model (Fig. 10, A and B). The neuroprotective effect of *tmc-1* also depends on the GABA and GABA receptors, as loss of function of either *rab-3* or *gbb-1* attenuates the effects of *tmc-1(OE)* (Fig. 10, A and B). Similar to neuronal aging, *pkc-1(lf)* animals suppress the locomotion phenotypes in this Alzheimer's disease model (*byIs161*) in the same manner as *tmc-1(OE)* animals (Fig. 10, A and B). We also found that PKC expression and activation levels were both increased in *byIs161* animals (fig. S11, C to E), suggesting that PKC may play a prodegeneration role in Tau-mediated Alzheimer's diseases. In summary, our results demonstrate that the TMC-1–GABA–PKC signaling axis may also play important roles in neurodegenerative disease conditions (Fig. 10C).

DISCUSSION

Neurons undergo metabolic and physiologic changes during aging, and this neuronal aging can be a cause or consequence of animal aging (*70*, *71*). Recent studies suggest that neuronal aging can be uncoupled from overall aging and regulated by neuron-specific mechanisms (*70*, *71*). In this study, we developed a new pipeline for studying neuronal proteomic profiles in vivo during aging. By comparing the neuronal proteomes in young and aged animals, we uncovered the anti-neuronal aging function of the conserved channel protein *tmc-1* in *C. elegans*. We further showed that *tmc-1* acts in GABAergic neurons to promote GABA release, and GABA can subsequently function outside of GABA synapses to activate metabotropic $GABA_B$ receptors. The activation of $GABA_B$ receptors then suppresses the activation of the PLCβ-PKC signaling to protect neurons from aging. The neuroprotective function of the TMC-1–GABA–PKC signaling axis is not only limited to neuronal aging, as activation of this signals axis can also suppress neuronal functional decline in a *C. elegans* Alzheimer's disease model. As the expression of the mouse *tmc-1* homolog can rescue the *tmc-1(lf)* neuronal aging phenotypes, and all key factors in this signaling axis are highly conserved across the animal kingdom, the findings we reported here are likely to be evolutionarily conserved.

The function of the TMC-1–GABA–PKC signaling axis does not appearthrough directlyregulating the insulin signal pathway, as loss of function in *daf-16*/FOXO, a key downstream transcriptional factor in the insulin pathway (*72*), only partially suppressed the neuroprotective function of *tmc-1(OE)*, and *tmc-1(OE)* did not affect DAF-16 protein level or localization (fig. S12, A to C). Our previous study showed that PVD neurons displayed aging-associated increase of autophagosomes, and suppression of the autophagy pathway delayed the onset of PVD degeneration during aging (*27*). To address the functional significance of the autophagy and mitophagy pathways in the TMC-1–GABA–PKC–mediated neuroprotection, we examined the effects of *tmc-1(OE)*, GABA supplements, and baclofen treatments. Our results showed that PVD neurons displayed aging-associated increased mitophagy in the similar fashion as that in autophagy (fig. S13). Activation of the TMC-1–GABA–PKC signaling axis by overexpressing TMC-1 or treating animals with GABA or baclofen all suppressed aging-associated increase of autophagy or mitophagy (fig. S13). These data suggested that activations of autophagy and mitophagy likely caused PVD neuronal aging, and the neuroprotective function of the TMC-1–GABA–PKC signaling axis might function through suppression of the autophagy and mitophagy pathways.

C. elegans tmc-1 has been shown to function in chemical and mechanical sensation, but it is also broadly expressed in many other neurons besides sensory neurons, if not in all neurons, suggesting that it may play other roles in the nervous system (*35*–*37*). The mammalian Tmc family contains eight genes and can be divided into three subfamilies, including one subfamily that contains Tmc1, Tmc2, and Tmc3 (*11*, *73*). Genetic and electrophysiological studies show that *C. elegans tmc-1* shares functional homology with

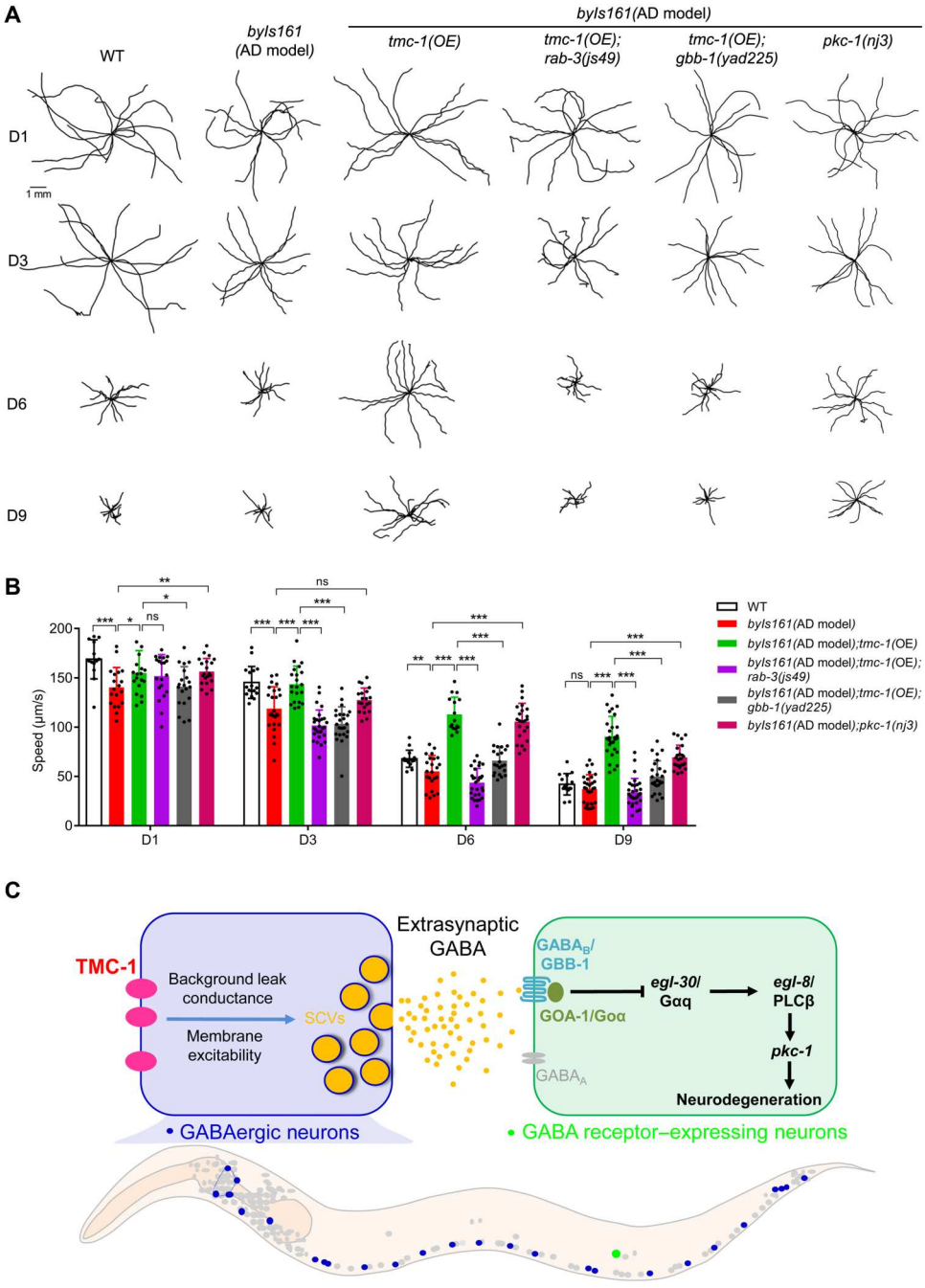

Fig. 10. Activation of the TMC-1–GABA–PKC signaling axis protects neurons in a *C. elegans* Alzheimer's disease model. (**A**) Representative 30-s locomotion trajectories superimposed for 12 animals of each experiment group as indicated. The starting points for each trajectory are aligned for clarity. Scale bar, 1 mm. (**B**) Average locomotion speed of animals. Data are presented as means ± SD of at least 15 animals. Student's *t* test for each time point, **P* < 0.05, ***P* < 0.01, ****P* < 0.001. (**C**) Model for the TMC-1–GABA–PKC signaling axis in neuronal aging and neurodegeneration.

mammalian Tmc1, Tmc2, and Tmc3 (*35*, *37*). Tmc1 is the most studied member of Tmc family proteins in mammals, and most of these studies are focused on the auditory system, where Tmc1 is believed to be the core components of the mechano-electrical transducer channel (*9*, *10*, *74*, *75*). However, Tmc1 has significant expression in many regions of the brain in rodents and human (Allen Brain Atlas, www.brain-map.org) (*11*, *73*), where its functions are still largely unknown. The broad expression of Tmc1 in human brain is observed not only in young individuals but also in aged ones (*76*). Recent results from analyses of gene expression patterns using more than 1800 human brain samples (ranging from 16 to 106 years old) from two large independent cohorts show that Tmc1 is one of the top 100 genes with aging-associated increased mRNA expression in the cerebellum (*76*). This

aging-associated increase of Tmc1 expression in human cerebellum is also confirmed by our analyses of Tmc1 protein levels, in which we examined three young and three aged healthy donors and found that Tmc1 had significant high expression in aged cerebellum when compared with younger ones (fig. S14, A to F). Results from immunostaining also showed the aging-associated increase of Tmc1 expression in neurons (fig. S14, D to F). The broad neuronal expression of *C. elegans tmc-1* and mammalian Tmc1 and their similarities in function and primary sequence, together with the same aging-associated increased expression in the brain, suggest that mammalian Tmc1 may play a similar role as *C. elegans tmc-1* during neuronal aging.

Vesicle release is a fundamental feature of neurons, and based on their size and appearance in electron micrographs, neuronal vesicles can be classified into two types: SCVs (40 to 60 nm diameter) and DCVs (60 to 120 nm diameter). SCVs contain classical neurotransmitters, and DCVs pack neuropeptides and biogenic amine neuromodulators. Recent studies highlight the functions of small peptides including insulin, neuropeptides, and antimicrobial peptides in regulating aging, which also suggests that DCVs, rather than SCVs, likely play more important roles in neuronal aging and animal aging (*1*, *27*). In this study, we show that *tmc-1* can regulate neuronal aging through release of SCVs but not DCVs, supporting a critical role of SCVs in neuronal aging. A previous study shows that neuronal SCVs are also required for unfolded protein response (UPR)–dependent regulation of *C. elegans* life span (*40*), supporting the role of SCVs beyond neuronal aging as well.

GABA is one of the major neuronal neurotransmitters, and most studies focus on the synaptic function of GABA. In this study, we show that extrasynaptic GABA plays important protective roles in neuronal aging. A recent study in *C. elegans* showed that dietary uptake of GABA could suppress stress-associated neurodegeneration (*77*), suggesting that GABA may have protective roles in many aspects of neuronal function. GABA mainly functions through GABA receptors, including ionotropic $GABA_A$ receptors and metabotropic $GABA_B$ receptors. $GABA_A$ receptors are chloride permanent channels, and activation of $GABA_A$ receptors causes hyperpolarization of cells. In the nervous system, GABA-$GABA_A$ functions as the major inhibitory signal to balance the function of neural circuits and is involved in most, if not all, functions of the brain (*78*, *79*). Different from $GABA_A$ receptors, $GABA_B$ receptors are G protein–coupled receptors that mediate a slow response to GABA. Although $GABA_B$ receptors can also regulate neuronal excitability, they mainly function by activating intracellular signals (*80*). However, compared with $GABA_A$ receptors, the function and regulation of $GABA_B$ receptors in the brain are not well studied. One interesting but perplexing observation regarding GABA and GABA receptors is that GABA receptors are expressed in many neurons that are not associated with GABAergic neurons in both vertebrates and invertebrates (*24*). Studies in *C. elegans* show that GABA receptors are expressed in nearly 90% of all neurons, and among them, more than 31% of the $GABA_A$ and 37% of the $GABA_B$ receptor–expressing neurons do not receive inputs from GABAergic neurons (*25*, *26*). All these observations suggest that GABA and GABA receptors may play a more important and widespread role in the brain than what was previously known, and the regulation between GABA and GABA receptors is not limited to synapses or within neuronal circuits. Through careful analyses of multiple types of *C. elegans* neurons that do not have direct inputs from GABAergic neurons, we show that extrasynaptic GABA plays a key role in many aging-associated neuronal phenotypes, such as neurodegeneration, locomotion decline, and axon regeneration decline, and this GABA function is mediated by metabotropic $GABA_B$ receptors through inhibition of the PKC pathway within neurons. The functions of extrasynaptic GABA and $GABA_B$ receptors in aging are not limited to the nervous system, because recent studies show that GABA and $GABA_B$ receptors can also regulate *C. elegans* life span (*52*, *81*). Therefore, it is possible that the TMC-1–GABA–PKC signaling axis described in this study may play a broader role beyond neuronal aging.

MATERIALS AND METHODS

C. elegans strains and plasmids generated in this study are available from the lead contact without restriction.

Lead contact

Further information and requests for resources should be directed to and will be fulfilled by the lead contact, D.Y. (dong.yan@duke.edu).

C. elegans strains and maintenance

C. elegans were maintained on nematode growth medium (NGM) with *E. coli* OP50 at 20°C as previously described (*82*) unless otherwise indicated. For the TurboID proximity labeling experiments, worms were fed on biotin auxotrophic *E. coli* (MG1655bioB: kan). For aging-associated experiments, age-synchronized animals were yielded by isolating eggs after bleach treatment as previously described. Wild-type strain was of the Bristol N2. Transgenic lines were generated by injection of plasmid DNA mixes into the hermaphrodite gonad. Integrated transgenic strains were generated with UV/trioxsalen treatment and then backcrossed with N2 two times. The *unc-18(yad172)* mutant was generated by CRISPR-Cas9 technology. All strains used in this study are listed in table S1.

Construction of transgenic strains and CRISPR-Cas9 genome editing

Transgenic strains were generated by microinjection. All plasmids used for microinjection were made by Gateway cloning technology. DNA fragments of specific genes and related promoters were amplified using polymerase chain reaction (PCR) and then inserted in pCR8 entry vector or destination vector, respectively. P*unc-122*::GFP (green fluorescent protein) or P*unc-122*::RFP (red fluorescent protein) were used as the coinjection marker.

CRISPR-Cas9 was used to generate the *unc-18(yad172)*, *gbb-1(yad225)*, and *gbb-2(yad227)* mutants and outlined as follows (*83*). The single-guide RNA (sgRNA) sequences of *unc-18* were designed on the basis of the target sequence characterized by G/A(N)19NGG, which was subsequently placed into the pU6::G/A(N)19_sgRNA plasmid by overlap extension PCR. sgRNA plasmids (50 ng/μl) were mixed with Cas9 expression plasmid (30 ng/μl) and coinjection marker (30 ng/μl) and were injected into wild-type worms to generate mutations. All recombinant DNAs are listed in table S2.

Biotin labeling with TurboID in *C. elegans*

yadIs83[P*rgef-1*::3×HA::TurboID,P*unc-122*::GFP], *yadIs112*[P*col-19*::3×HA::TurboID,P*unc-122*::GFP], and *yadIs118*[P*myo-*

3::3×HA::TurboID,P*unc-122*::GFP] were generated to specifically express TurboID in neurons, hypodermis, and muscles, respectively. Animals used for TurboID proximity labeling were grown on biotin auxotrophic *E. coli* (MG1655) for at least two generations to deplete excessive biotin. A total of 6000 synchronized L1 were seeded on MG1655 NGM plates and grown to L4 stage at 20°C. L4-stage animals were transferred on MG1655 NGM plates with FUDR (5-fluoro-2-deoxyuridine; 100 μg/ml) for proximity labeling during aging. At each time point during aging, 300 μM exogenous biotin was added in the MG1655 NGM plates with the animals and cultured at 25°C for 8 hours before whole-animal lysis. Subsequently, animals were collected on ice and washed three times with M9 buffer and finally in radioimmunoprecipitation assay (RIPA) buffer for sonication while always being kept on ice. The lysates were centrifuged at 10,000*g* at 4°C to remove the debris and lipids. The supernatants were used for enrichment by streptavidin-coated beads or Western blot analysis.

Biotinylated protein enrichment with streptavidin-coated beads

To enrich biotinylated proteins, 100 μl of streptavidin-coated magnetic beads was washed twice with RIPA buffer, incubated with clarified lysates for each sample, and rotated overnight at 4°C. The beads were subsequently washed twice with 1 ml of RIPA buffer, once with 1 ml of 1 M KCl, once with 1 ml of 0.1 M Na_2CO_3, once with 1 ml of 2 M urea in 10 mM tris-HCl (pH 8.0), and twice with 1 ml of RIPA buffer. Last, the washed beads were suspended in 120 μl of elution buffer (2% SDS, 25 mM tris-HCl, 50 mM NaCl, 2 mM biotin, and 20 mM dithiothreitol). Biotinylated proteins were then eluted from the beads by boiling the beads in elution buffer. For each sample, 20 μl of eluates was mixed with protein sample buffer for Western blot analysis, and the remaining 100 μl of eluates was used for high-performance liquid chromatography–mass spectrometry (HPLC-MS) analysis.

Quantitative LC-MS/MS analysis

Quantitative LC-MS/MS was performed on 2 μl of each sample, using a nanoAcquity UPLC system (Waters Corp.) coupled to a Thermo Orbitrap Fusion Lumos high-resolution accurate mass tandem mass spectrometer (Thermo Fisher Scientific) via a nanoelectrospray ionization source. Briefly, the sample was first trapped on a Symmetry C18 20 mm × 180 μm trapping column [5 μl/min at 99.9/0.1 (v/v) water/acetonitrile], after which the analytical separation was performed using a 1.8-μm Acquity HSS T3 C18 75 μm × 250 mm column (Waters Corp.) with a 90-min linear gradient of 5 to 30% acetonitrile with 0.1% formic acid at a flow rate of 400 nl/min with a column temperature of 55°C. Data collection on the Fusion Lumos mass spectrometer was performed in a data-dependent acquisition mode of acquisition with an r = 120,000 [at mass/charge ratio (m/z) 200] full-MS scan from m/z 375 to 1500 with a target automatic gain control (AGC) value of 2×10^5 ions. MS/MS scans were acquired at rapid scan rate (ion trap) with an AGC target of 5×10^3 ions and a maximum injection time of 100 ms. The total cycle time for MS and MS/MS scans was 2 s. A 20-s dynamic exclusion was used to increase depth of coverage. The total analysis cycle time for each sample injection was approximately 2 hours. Following all UPLC-MS/MS analyses, data were imported into Proteome Discoverer 2.4 (Thermo Fisher Scientific Inc.), and analyses were aligned on the basis of the accurate mass and retention time of detected ions ("features") using Minora Feature Detector algorithm in Proteome Discoverer. Relative peptide abundance was calculated on the basis of area under the curve (AUC) of the selected ion chromatograms of the aligned features across all runs. The MS/MS data were searched against the *C. elegans* database (downloaded in April 2018), an equal number of reversed-sequence "decoys" for false discovery rate determination. Mascot Distiller and Mascot Server (v 2.5, Matrix Sciences) were used to produce fragment ion spectra and to perform the database searches. Data were searched at 5 parts per million (ppm) precursor and 0.8 Da product mass accuracy with full trypsin enzyme rules. Database search parameters included fixed modification on Cys (carbamidomethyl) and variable modifications on Meth (oxidation) and Asn and Gln (deamidation). Peptide Validator and Protein FDR Validator nodes in Proteome Discoverer were used to annotate the data at a maximum 1% protein false discovery rate.

Proteomic data analysis

Protein abundances were calculated on the basis of the normalized raw data from quantitative LC-MS/MS. On the basis of these values, DESeq2 (*84*) was used to determine differential expression of proteins among time points and tissues. In brief, DESeq2 was used to transform counts using the variance-stabilizing method to account for nonindependence of variance on the mean and then data were fit into the negative binomial distribution. Log_2 fold change and Wald test P values were calculated for each protein for pairwise time points. Batch effects from multiple experiments were corrected using the removeBatchEffect function from the limma package (*85*). P values from DESeq2 underwent multiple comparison correction using Benjamini-Hochberg procedure to minimize false discovery rate. Venn diagrams were generated to compare the number of differentially expressed proteins among pairwise time points using the R ggVennDiagram package (https://github.com/gaospecial/ggVennDiagram). To detect possible overall proteomic structure in all samples, we used principal components analysis. This analysis was conducted on batch-corrected normalized values for the top 1500 expressed proteins across all samples and values from DESeq2. Gene pathway enrichment analysis on differentially expressed proteins was performed using STRING.

Quantification of PVD/ALM/PLM neuron degeneration

wdIs51[F49H12.4::GFP + *unc-119(+)*] and *zdIs5*[*mec-4p::GFP* + *lin-15(+)*] were used for observation of PVD/ALM/PLM neuronal aging. The PVD/ALM/PLM aging was quantified using ×63 magnification on the ZESS microscope as previously described (*27*, *28*). Degenerated PVD neurons will show bubble- and bead-like structures on the PVD dendrite. In aged animals, the ALM neurons will exhibit soma outgrowth and PLM neurons will present wavy and acute bends on anterior processes/dendrites. For each independent experiment, at least 50 animals were used for quantification of neuron degeneration. Three to four replicates were conducted for each experiment.

Western blot analysis

Worms were collected in M9 buffer from NGM plates and quickly washed several times. *C. elegans* or human tissues were suspended in RIPA buffer for sonication and always kept on ice. The lysates after sonication were centrifuged at 10,000*g* at 4°C to remove the debris and lipids. The supernatants were mixed with equal

amounts of protein sample buffer and denatured for 5 min at 95°C. Denatured protein samples were loaded and separated by 4 to 20% SDS–polyacrylamide gel electrophoresis gel (Bio-Rad) and then transferred to polyvinylidene difluoride membranes. The primary antibodies were rabbit anti-HA (hemagglutinin) antibody (Sigma-Aldrich, H6908), anti-TMC1 (Abcam, ab199949), rabbit anti-Phospho-PKC Substrate Motif [(R/K)XpSX(R/K)] MultiMab antibody mix (Cell Signaling Technology, #6967), mouse anti-PKC (Santa Cruz Biotechnology, sc-17769), and rabbit anti-actin (Sigma-Aldrich, A2066) at 1:1000 dilution. The secondary antibody was goat anti-rabbit immunoglobulin G (IgG) at 1:5000 dilution (GE Healthcare). Biotinylated proteins were blotted using horseradish peroxidase–conjugated streptavidin (Thermo Fisher Scientific, N100).

Chemicals

GABA (A2129, Sigma-Aldrich) was diluted in water to 100 mM stocks, which were diluted in NGM to a final concentration of 200 μM before transferring animals on. Bicuculline (14340, Sigma-Aldrich) and gabazine (S106, Sigma-Aldrich) are two antagonists of $GABA_A$ receptor, which are diluted in NGM to a final concentration of 250 μM for treatment. Saclofen (S166, Sigma-Aldrich) is antagonist of $GABA_B$ receptor, which is diluted in NGM to a final concentration of 200 μM for treatment. Baclofen (B5399, Sigma-Aldrich) is a $GABA_B$ agonist, which is diluted in NGM to 250 μM to treat animals for PVD degeneration analysis, PLM neuron regeneration analysis, and locomotion analysis.

Visualization and quantification of fluorescence

Worms were picked and mounted on a 4% agarose pad. For neurodegeneration quantification, animals were observed without applying any anesthetics. For other fluorescence observation, animals were anesthetized with 1% 1-phenoxy-2-propanol (TCI America) in M9 buffer. Fluorescence was visualized under a Zeiss fluorescence microscope and a Zeiss LSM700 confocal microscope. The fluorescence intensity was quantified by Fiji (ImageJ).

Locomotion and behavior assays

The locomotion analysis was performed as previously described (*50*, *86*). Young or aged animals were picked on the NGM plates without any food. After 5 to 10 min, a 30-s video for individual animals was captured using a Leica stereomicroscope with a camera (Leica MC120 HD). Each animal in the video was analyzed by Fiji (ImageJ) with the TrackMate plugin. The data of locomotion trajectory and speed for each animal were produced from frame by frame analysis in Fiji. Twenty or more animals were used for each experiment. To superimpose the locomotion trajectories together, the starting points for each trajectory were aligned to the 0 point of axis.

Laser axotomy

zdIs5 [*mec-4p::GFP*] was used to perform axotomy as previously described (*87*). Animals were immobilized by using 5 mM levamisole (Sigma-Aldrich) in M9 buffer on an agar pad. We cut PLM axons on the Zeiss fluorescence microscope with a 435-nm MicroPoint Laser System (laser dye cells, MP-27-435-DYE) (*88*) and subsequently transferred the animal onto an NGM plate. Animals were anesthetized for confocal imaging at the PLM region 24 hours after axotomy.

Immunostaining

Worms were collected in 1 ml of M9 buffer and washed three times to get rid of bacteria. After M9 washing, animals were fixed with 1% paraformaldehyde for 30 min at room temperature. The fixed worm bodies were washed twice using TBB buffer [100 mM tris-HCl (pH 7.4), 1% Triton X-100, and 1 mM EDTA] and rotated in 5% β-mercaptoethanol overnight. Then, worm bodies were incubated in order with blocking buffer (1.5% bovine serum albumin, 1.5% normal goat serum, 0.5% Triton, and 0.05% NaN_3 in phosphate-buffered saline), rabbit anti-HA antibody (Sigma-Aldrich, H6908), and goat anti-rabbit IgG Alexa Fluor 568 (Life Technologies, A11011). Immunostaining images were captured by the Zeiss LSM700 confocal microscope.

Immunofluorescence staining of paraffin sections

Immunofluorescence staining was performed on formalin-fixed, paraffin-embedded tissue sections using a rabbit monoclonal antibody to TMC-1 (Abcam, ab199949). Sections were deparaffinized according to established procedures (20 min in xylenes, 10 min in 100% ethanol, 10 min in 95% ethanol, and 10 min in dH_2O). After washing in water, sections were blocked with Sudan black (0.1% SSB in 70% ethanol) for 5 min and then cleared with water for 10 min. Antigen retrieval was performed with boiling citrate buffer (pH 6.0) for 20 min. Slides were rinsed and washed in water for 10 min and cultured with blocking buffer (10% normal goat serum in primary antibody buffer) at room temperature overnight. After washing in water for 10 min, the sections were incubated with the primary antibodies (1:500) at 4°C overnight. The next day, the primary antibody was removed using water and the fresh primary antibody was applied for 4 hours at room temperature. Slides were rinsed and washed in water for 10 min and cultured with secondary antibody (Invitrogen, Alexa Fluor 488 goat anti-rabbit IgG) at room temperature for 1 hour. After washing in water for 10 min, slides were mounted and imaged with a confocal microscope.

Life span assay

Life span assays were performed under 20°C. Age-synchronized animals were acquired as described above. For each strain, 240 L4-stage animals were transferred on three fresh NGM plates with FUDR (100 μg/ml). Survival of the animals was examined every 1 to 2 days. Animals that do not respond to mechanical prodding were scored as dead.

Statistical analysis

Data are presented as means ± SD unless specifically indicated. Statistical analyses included *t* test or one-way analysis of variance. All figures were generated using GraphPad Prism 7 (GraphPad Software, La Jolla, CA, USA), BioEdit, and Adobe Illustrator.

Supplementary Materials

This PDF file includes:
Figs. S1 to S14
Tables S1 and S2

Other Supplementary Material for this manuscript includes the following:
Table S3 and S4

View/request a protocol for this paper from *Bio-protocol*.

REFERENCES AND NOTES

1. J. V. Pluvinage, T. Wyss-Coray, Systemic factors as mediators of brain homeostasis, ageing and neurodegeneration. *Nat. Rev. Neurosci.* **21**, 93–102 (2020).
2. Y. Hou, X. Dan, M. Babbar, Y. Wei, S. G. Hasselbalch, D. L. Croteau, V. A. Bohr, Ageing as a risk factor for neurodegenerative disease. *Nat. Rev. Neurol.* **15**, 565–581 (2019).
3. Ageing - United Nations report on world population ageing. *World Today* **58**, 12–13 (2002).
4. F. Sierra, E. Hadley, R. Suzman, R. Hodes, Prospects for life span extension. *Annu. Rev. Med.* **60**, 457–469 (2009).
5. C. Peng, J. Q. Trojanowski, V. M. Lee, Protein transmission in neurodegenerative disease. *Nat. Rev. Neurol.* **16**, 199–212 (2020).
6. R. Stark, M. Grzelak, J. Hadfield, RNA sequencing: The teenage years. *Nat. Rev. Genet.* **20**, 631–656 (2019).
7. C. Buccitelli, M. Selbach, mRNAs, proteins and the emerging principles of gene expression control. *Nat. Rev. Genet.* **21**, 630–644 (2020).
8. T. C. Branon, J. A. Bosch, A. D. Sanchez, N. D. Udeshi, T. Svinkina, S. A. Carr, J. L. Feldman, N. Perrimon, A. Y. Ting, Efficient proximity labeling in living cells and organisms with TurboID. *Nat. Biotechnol.* **36**, 880–887 (2018).
9. S. Liu, S. Wang, L. Zou, J. Li, C. Song, J. Chen, Q. Hu, L. Liu, P. Huang, W. Xiong, TMC1 is an essential component of a leak channel that modulates tonotopy and excitability of auditory hair cells in mice. *eLife* **8**, e47441 (2019).
10. Y. Jia, Y. Zhao, T. Kusakizako, Y. Wang, C. Pan, Y. Zhang, O. Nureki, M. Hattori, Z. Yan, TMC1 and TMC2 proteins are pore-forming subunits of mechanosensitive ion channels. *Neuron* **105**, 310–321.e3 (2020).
11. K. Kurima, Y. Yang, K. Sorber, A. J. Griffith, Characterization of the transmembrane channel-like (TMC) gene family: Functional clues from hearing loss and epidermodysplasia verruciformis. *Genomics* **82**, 300–308 (2003).
12. T. G. Smart, F. A. Stephenson, A half century of γ-aminobutyric acid. *Brain Neurosci. Adv.* **3**, 2398212819858249 (2019).
13. E. Florey, GABA: History and perspectives. *Can. J. Physiol. Pharmacol.* **69**, 1049–1056 (1991).
14. E. M. Jorgensen, GABA, in *WormBook: The Online Review of* C. elegans *Biology*, (WormBook, 2005) pp. 1–13.
15. C. Maes, L. Hermans, L. Pauwels, S. Chalavi, I. Leunissen, O. Levin, K. Cuypers, R. Peeters, S. Sunaert, D. Mantini, N. A. J. Puts, R. A. E. Edden, S. P. Swinnen, Age-related differences in GABA levels are driven by bulk tissue changes. *Hum. Brain Mapp.* **39**, 3652–3662 (2018).
16. E. C. Porges, A. J. Woods, R. A. E. Edden, N. A. J. Puts, A. D. Harris, H. Chen, A. M. Garcia, T. R. Seider, D. G. Lamb, J. B. Williamson, R. A. Cohen, Frontal gamma-aminobutyric acid concentrations are associated with cognitive performance in older adults. *Biol. Psychiatry Cogn. Neurosci. Neuroimaging* **2**, 38–44 (2017).
17. J. D. Chamberlain, H. Gagnon, P. Lalwani, K. E. Cassady, M. Simmonite, R. D. Seidler, S. F. Taylor, D. H. Weissman, D. C. Park, T. A. Polk, GABA levels in ventral visual cortex decline with age and are associated with neural distinctiveness. *Neurobio. Aging* **102**, 170–177 (2021).
18. T. Hua, C. Kao, Q. Sun, X. Li, Y. Zhou, Decreased proportion of GABA neurons accompanies age-related degradation of neuronal function in cat striate cortex. *Brain Res. Bull.* **75**, 119–125 (2008).
19. A. G. Leventhal, Y. Wang, M. Pu, Y. Zhou, Y. Ma, GABA and its agonists improved visual cortical function in senescent monkeys. *Science* **300**, 812–815 (2003).
20. N. Cawley, B. S. Solanky, N. Muhlert, C. Tur, R. A. E. Edden, C. A. M. Wheeler-Kingshott, D. H. Miller, A. J. Thompson, O. Ciccarelli, Reduced gamma-aminobutyric acid concentration is associated with physical disability in progressive multiple sclerosis. *Brain* **138**, 2584–2595 (2015).
21. W. Sieghart, Structure, pharmacology, and function of GABAA receptor subtypes. *Adv. Pharmacol.* **54**, 231–263 (2006).
22. H. Shaye, B. Stauch, C. Gati, V. Cherezov, Molecular mechanisms of metabotropic GABAB receptor function. *Science Adv.* **7**, eabg3362 (2021).
23. D. J. Laurie, W. Wisden, P. H. Seeburg, The distribution of thirteen GABAA receptor subunit mRNAs in the rat brain. III. Embryonic and postnatal development. *J. Neurosci.* **12**, 4151–4172 (1992).
24. J. S. Barker, R. M. Hines, Regulation of GABAA receptor subunit expression in substance use disorders. *Int. J. Mol. Sci.* **21**, 4445 (2020).
25. M. Gendrel, E. G. Atlas, O. Hobert, A cellular and regulatory map of the GABAergic nervous system of C. elegans. *eLife* **5**, e17686 (2016).
26. E. Yemini, A. Lin, A. Nejatbakhsh, E. Varol, R. Sun, G. E. Mena, A. D. T. Samuel, L. Paninski, V. Venkatachalam, O. Hobert, NeuroPAL: A multicolor atlas for whole-brain neuronal identification in C. elegans. *Cell* **184**, 272–288.e11 (2021).
27. E. Lezi, T. Zhou, S. Koh, M. Chuang, R. Sharma, N. Pujol, A. D. Chisholm, C. Eroglu, H. Matsunami, D. Yan, An antimicrobial peptide and its neuronal receptor regulate dendrite degeneration in aging and infection. *Neuron* **97**, 125–138.e5 (2018).
28. M. L. Toth, I. Melentijevic, L. Shah, A. Bhatia, K. Lu, A. Talwar, H. Naji, C. Ibanez-Ventoso, P. Ghose, A. Jevince, J. Xue, L. A. Herndon, G. Bhanot, C. Rongo, D. H. Hall, M. Driscoll, Neurite sprouting and synapse deterioration in the aging Caenorhabditis elegans nervous system. *J. Neurosci.* **32**, 8778–8790 (2012).
29. K. K. Steffen, A. Dillin, A ribosomal perspective on proteostasis and aging. *Cell Metab.* **23**, 1004–1012 (2016).
30. A. S. Anisimova, A. I. Alexandrov, N. E. Makarova, V. N. Gladyshev, S. E. Dmitriev, Protein synthesis and quality control in aging. *Aging (Albany NY)* **10**, 4269–4288 (2018).
31. J. G. White, E. Southgate, J. N. Thomson, S. Brenner, The structure of the nervous system of the nematode Caenorhabditis elegans. *Philos. Trans. R. Soc. Lond. B Biol. Sci.* **314**, 1–340 (1986).
32. C. L. Pan, C. Y. Peng, C. H. Chen, S. McIntire, Genetic analysis of age-dependent defects of the Caenorhabditis elegans touch receptor neurons. *Proc. Natl. Acad. Sci. U.S.A.* **108**, 9274–9279 (2011).
33. C. Ising, M. T. Heneka, Functional and structural damage of neurons by innate immune mechanisms during neurodegeneration. *Cell Death Dis.* **9**, 120 (2018).
34. F. M. Menzies, A. Fleming, A. Caricasole, C. F. Bento, S. P. Andrews, A. Ashkenazi, J. Füllgrabe, A. Jackson, M. Jimenez Sanchez, C. Karabiyik, F. Licitra, A. Lopez Ramirez, M. Pavel, C. Puri, M. Renna, T. Ricketts, L. Schlotawa, M. Vicinanza, H. Won, Y. Zhu, J. Skidmore, D. C. Rubinsztein, Autophagy and neurodegeneration: Pathogenic mechanisms and therapeutic opportunities. *Neuron* **93**, 1015–1034 (2017).
35. X. Yue, J. Zhao, X. Li, Y. Fan, D. Duan, X. Zhang, W. Zou, Y. Sheng, T. Zhang, Q. Yang, J. Luo, S. Duan, R. Xiao, L. Kang, TMC proteins modulate egg laying and membrane excitability through a background leak conductance in C. elegans. *Neuron* **97**, 571–585.e5 (2018).
36. M. Chatzigeorgiou, S. Bang, S. W. Hwang, W. R. Schafer, tmc-1 encodes a sodium-sensitive channel required for salt chemosensation in C. elegans. *Nature* **494**, 95–99 (2013).
37. X. Wang, G. Li, J. Liu, J. Liu, X. Z. Xu, TMC-1 mediates alkaline sensation in C. elegans through nociceptive neurons. *Neuron* **91**, 146–154 (2016).
38. M. Driscoll, M. Chalfie, The mec-4 gene is a member of a family of Caenorhabditis elegans genes that can mutate to induce neuronal degeneration. *Nature* **349**, 588–593 (1991).
39. S. Speese, M. Petrie, K. Schuske, M. Ailion, K. Ann, K. Iwasaki, E. M. Jorgensen, T. F. J. Martin, UNC-31 (CAPS) is required for dense-core vesicle but not synaptic vesicle exocytosis in Caenorhabditis elegans. *J. Neurosci.* **27**, 6150–6162 (2007).
40. R. C. Taylor, A. Dillin, XBP-1 is a cell-nonautonomous regulator of stress resistance and longevity. *Cell* **153**, 1435–1447 (2013).
41. Y. Hata, C. A. Slaughter, T. C. Südhof, Synaptic vesicle fusion complex contains unc-18 homologue bound to syntaxin. *Nature* **366**, 347–351 (1993).
42. M. L. Nonet, J. E. Staunton, M. P. Kilgard, T. Fergestad, E. Hartwieg, H. R. Horvitz, E. M. Jorgensen, B. J. Meyer, Caenorhabditis elegans rab-3 mutant synapses exhibit impaired function and are partially depleted of vesicles. *J. Neurosci.* **17**, 8061–8073 (1997).
43. O. Saifee, L. Wei, M. L. Nonet, The Caenorhabditis elegans unc-64 locus encodes a syntaxin that interacts genetically with synaptobrevin. *Mol. Biol. Cell* **9**, 1235–1252 (1998).
44. Z. W. Wang, O. Saifee, M. L. Nonet, L. Salkoff, SLO-1 potassium channels control quantal content of neurotransmitter release at the C-. elegans neuromuscular junction. *Neuron* **32**, 867–881 (2001).
45. R. Kerr, V. Lev-Ram, G. Baird, P. Vincent, R. Y. Tsien, W. R. Schafer, Optical imaging of calcium transients in neurons and pharyngeal muscle of C-elegans. *Neuron* **26**, 583–594 (2000).
46. O. Hobert, The neuronal genome of *Caenorhabditis elegans*, in *WormBook: The Online Review of* C. elegans *Biology*, (WormBook, 2013) pp. 1–106.
47. Y. Jin, E. Jorgensen, E. Hartwieg, H. R. Horvitz, The Caenorhabditis elegans gene unc-25 encodes glutamic acid decarboxylase and is required for synaptic transmission but not synaptic development. *J. Neurosci.* **19**, 539–548 (1999).
48. C. Eastman, H. R. Horvitz, Y. Jin, Coordinated transcriptional regulation of the unc-25 glutamic acid decarboxylase and the unc-47 GABA vesicular transporter by the Caenorhabditis elegans UNC-30 homeodomain protein. *J. Neurosci.* **19**, 6225–6234 (1999).
49. P. Liu, B. Chen, Z. W. Wang, GABAergic motor neurons bias locomotor decision-making in C. elegans. *Nat. Commun.* **11**, 5076 (2020).
50. J. S. Dittman, J. M. Kaplan, Behavioral impact of neurotransmitter-activated G-protein-coupled receptors: Muscarinic and GABAB receptors regulate Caenorhabditis elegans locomotion. *J. Neurosci.* **28**, 7104–7112 (2008).
51. C. Darby, S. Falkow, Mimicry of a G protein mutation by pertussis toxin expression in transgenic Caenorhabditis elegans. *Infect. Immun.* **69**, 6271–6275 (2001).
52. L. Chun, J. Gong, F. Yuan, B. Zhang, H. Liu, T. Zheng, T. Yu, X. Z. S. Xu, J. Liu, Metabotropic GABA signalling modulates longevity in C. elegans. *Nat. Commun.* **6**, 8828 (2015).
53. B. Perez-Mansilla, S. Nurrish, Chapter 4 A network of G-protein signaling pathways control neuronal activity in C. elegans. *Adv. Genet.* **65**, 145–192 (2009).

54. B. Ravi, J. Zhao, S. I. Chaudhry, R. Signorelli, M. Bartole, R. J. Kopchock III, C. Guijarro, J. M. Kaplan, L. Kang, K. M. Collins, Presynaptic Gαo (GOA-1) signals to depress command neuron excitability and allow stretch-dependent modulation of egg laying in Caenorhabditis elegans. *Genetics* **218**, iyab080 (2021).
55. H. Yu, B. Aleman-Meza, S. Gharib, M. K. Labocha, C. J. Cronin, P. W. Sternberg, W. Zhong, Systematic profiling of Caenorhabditis elegans locomotive behaviors reveals additional components in G-protein Gαq signaling. *Proc. Natl. Acad. Sci. U.S.A.* **110**, 11940–11945 (2013).
56. D. S. Walker, R. P. Vázquez-Manrique, N. J. D. Gower, E. Gregory, W. R. Schafer, H. A. Baylis, Inositol 1,4,5-trisphosphate signalling regulates the avoidance response to nose touch in Caenorhabditis elegans. *PLOS Genet.* **5**, e1000636 (2009).
57. C. Bastiani, J. Mendel, Heterotrimeric G proteins in *C. elegans*, in *WormBook: The Online Review of* C. elegans *Biology* (WormBook, 2006) pp. 1–25.
58. A. Ghosh-Roy, Z. Wu, A. Goncharov, Y. Jin, A. D. Chisholm, Calcium and cyclic AMP promote axonal regeneration in Caenorhabditis elegans and require DLK-1 kinase. *J. Neurosci.* **30**, 3175–3183 (2010).
59. K. Goto, Y. Hozumi, T. Nakano, S. Saino-Saito, A. M. Martelli, Lipid messenger, diacylglycerol, and its regulator, diacylglycerol kinase, in cells, organs, and animals: History and perspective. *Tohoku J. Exp. Med.* **214**, 199–212 (2008).
60. I. Mérida, A. Avila-Flores, E. Merino, Diacylglycerol kinases: At the hub of cell signalling. *Biochem. J.* **409**, 1–18 (2008).
61. D. Sieburth, J. M. Madison, J. M. Kaplan, PKC-1 regulates secretion of neuropeptides. *Nat. Neurosci.* **10**, 49–57 (2007).
62. M. Zhen, A. D. Samuel, C. elegans locomotion: Small circuits, complex functions. *Curr. Opin. Neurobiol.* **33**, 117–126 (2015).
63. C. Huang, C. Xiong, K. Kornfeld, Measurements of age-related changes of physiological processes that predict lifespan of Caenorhabditis elegans. *Proc. Natl. Acad. Sci. U.S.A.* **101**, 8084–8089 (2004).
64. L. A. Herndon, P. J. Schmeissner, J. M. Dudaronek, P. A. Brown, K. M. Listner, Y. Sakano, M. C. Paupard, D. H. Hall, M. Driscoll, Stochastic and genetic factors influence tissue-specific decline in ageing C. elegans. *Nature* **419**, 808–814 (2002).
65. R. Kaletsky, V. Lakhina, R. Arey, A. Williams, J. Landis, J. Ashraf, C. T. Murphy, The C. elegans adult neuronal IIS/FOXO transcriptome reveals adult phenotype regulators. *Nature* **529**, 92–96 (2016).
66. L. DeVault, T. Li, S. Izabel, K. L. Thompson-Peer, L. Y. Jan, Y. N. Jan, Dendrite regeneration of adult *Drosophila* sensory neurons diminishes with aging and is inhibited by epidermal-derived matrix metalloproteinase 2. *Genes Dev.* **32**, 402–414 (2018).
67. L. Chen, Z. Wang, A. Ghosh-Roy, T. Hubert, D. Yan, S. O'Rourke, B. Bowerman, Z. Wu, Y. Jin, A. D. Chisholm, Axon regeneration pathways identified by systematic genetic screening in C. elegans. *Neuron* **71**, 1043–1057 (2011).
68. L. Gan, M. R. Cookson, L. Petrucelli, A. R. La Spada, Converging pathways in neurodegeneration, from genetics to mechanisms. *Nat. Neurosci.* **21**, 1300–1309 (2018).
69. C. Fatouros, G. J. Pir, J. Biernat, S. P. Koushika, E. Mandelkow, E. M. Mandelkow, E. Schmidt, R. Baumeister, Inhibition of tau aggregation in a novel Caenorhabditis elegans model of tauopathy mitigates proteotoxicity. *Hum. Mol. Genet.* **21**, 3587–3603 (2012).
70. A. Satoh, S. I. Imai, L. Guarente, The brain, sirtuins, and ageing. *Nat. Rev. Neurosci.* **18**, 362–374 (2017).
71. J. M. Zullo, D. Drake, L. Aron, P. O'Hern, S. C. Dhamne, N. Davidsohn, C. A. Mao, W. H. Klein, A. Rotenberg, D. A. Bennett, G. M. Church, M. P. Colaiácovo, B. A. Yankner, Regulation of lifespan by neural excitation and REST. *Nature* **574**, 359–364 (2019).
72. N. Libina, J. R. Berman, C. Kenyon, Tissue-specific activities of C. elegans DAF-16 in the regulation of lifespan. *Cell* **115**, 489–502 (2003).
73. G. Keresztes, H. Mutai, S. Heller, TMC and EVER genes belong to a larger novel family, the TMC gene family encoding transmembrane proteins. *BMC Genomics* **4**, 24 (2003).
74. M. Beurg, A. Barlow, D. N. Furness, R. Fettiplace, A *Tmc1* mutation reduces calcium permeability and expression of mechanoelectrical transduction channels in cochlear hair cells. *Proc. Natl. Acad. Sci. U.S.A.* **116**, 20743–20749 (2019).
75. K. Kurima, S. Ebrahim, B. Pan, M. Sedlacek, P. Sengupta, B. A. Millis, R. Cui, H. Nakanishi, T. Fujikawa, Y. Kawashima, B. Y. Choi, K. Monahan, J. R. Holt, A. J. Griffith, B. Kachar, TMC1 and TMC2 localize at the site of mechanotransduction in mammalian inner ear hair cell stereocilia. *Cell Rep.* **12**, 1606–1617 (2015).
76. L. Soreq; UK Brain Expression Consortium; North American Brain Expression Consortium, Major shifts in glial regional identity are a transcriptional hallmark of human brain aging. J. Rose, E. Soreq, J. Hardy, D. Trabzuni, M. R. Cookson, C. Smith, M. Ryten, R. Patani, J. Ule, *Cell Rep.* **18**, 557–570 (2017).
77. A. Urrutia, V. A. García-Angulo, A. Fuentes, M. Caneo, M. Legüe, S. Urquiza, S. E. Delgado, J. Ugalde, P. Burdisso, A. Calixto, Bacterially produced metabolites protect C. elegans neurons from degeneration. *PLOS Biol.* **18**, e3000638 (2020).
78. T. C. Jacob, S. J. Moss, R. Jurd, GABA(A) receptor trafficking and its role in the dynamic modulation of neuronal inhibition. *Nat. Rev. Neurosci.* **9**, 331–343 (2008).
79. B. Luscher, T. Fuchs, C. L. Kilpatrick, GABAA receptor trafficking-mediated plasticity of inhibitory synapses. *Neuron* **70**, 385–409 (2011).
80. M. Gassmann, B. Bettler, Regulation of neuronal GABA(B) receptor functions by subunit composition. *Nat. Rev. Neurosci.* **13**, 380–394 (2012).
81. F. Yuan, J. Zhou, L. Xu, W. Jia, L. Chun, X. Z. S. Xu, J. Liu, GABA receptors differentially regulate life span and health span in *C. elegans* through distinct downstream mechanisms. *Am. J. Physiol. Cell Physiol.* **317**, C953–C963 (2019).
82. S. Brenner, The genetics of Caenorhabditis elegans. *Genetics* **77**, 71–94 (1974).
83. A. E. Friedland, Y. B. Tzur, K. M. Esvelt, M. P. Colaiácovo, G. M. Church, J. A. Calarco, Heritable genome editing in C. elegans via a CRISPR-Cas9 system. *Nat. Methods* **10**, 741–743 (2013).
84. M. I. Love, W. Huber, S. Anders, Moderated estimation of fold change and dispersion for RNA-seq data with DESeq2. *Genome Biol.* **15**, 550 (2014).
85. M. E. Ritchie, B. Phipson, D. Wu, Y. Hu, C. W. Law, W. Shi, G. K. Smyth, limma powers differential expression analyses for RNA-sequencing and microarray studies. *Nucleic Acids Res.* **43**, e47 (2015).
86. Z. Hu, X. J. Tong, J. M. Kaplan, UNC-13L, UNC-13S, and Tomosyn form a protein code for fast and slow neurotransmitter release in Caenorhabditis elegans. *eLife* **2**, e00967 (2013).
87. D. Yan, Y. Jin, Regulation of DLK-1 kinase activity by calcium-mediated dissociation from an inhibitory isoform. *Neuron* **76**, 534–548 (2012).
88. M. Hammarlund, P. Nix, L. Hauth, E. M. Jorgensen, M. Bastiani, Axon regeneration requires a conserved MAP kinase pathway. *Science* **323**, 802–806 (2009).

Acknowledgments: We thank J. E. Cronan for the biotin-auxotrophic *E. coli* strain (MG1655); L. Chun and S. Xu for GABA regents; A. Zhang, Z. Qu, E. Lezi, Y. Jin, and J. Schneider for comments on the manuscript; and all other D.Y. laboratory members for double-blind experiments. Undergraduate student A. Swaine and C. Herman prepared most of the reagents used in this study. **Funding:** This project is supported by NIH grants NS105638 and AG073994 (to D.Y.). Some strains were provided by the CGC, which is funded by the NIH Office of Research Infrastructure Programs (P40 OD010440). Human samples in this study were provided by Duke/UNC Alzheimer's Disease Research Center, which is supported by grant P30AG072958. **Author contributions:** D.Y. devised the whole project. J.W. performed all molecular, genetic, and imaging experiments. E.S. carried out proteomics. L.W. and D.K. analyzed proteomic data with the help of J.W. J.F.E., S.-H.J.W., and J.W. carried out Tmc1 analyses in human samples. J.W. and D.Y. wrote the manuscript with inputs from all authors. **Competing interests:** The authors declare that they have no competing interests. **Data and materials availability:** All data needed to evaluate the conclusions in the paper are present in the paper and/or the Supplementary Materials.

Submitted 9 May 2022
Accepted 4 November 2022
Published 21 December 2022
10.1126/sciadv.adc9236